Energy Dependence of Proton Inelastic Scattering from ^{40}Ca†

C. R. Gruhn,* T. Y. T. Kuo,‡ C. J. Maggiore,§ H. McManus, F. Petrovich,¶ and B. M. Preedom‖
Department of Physics and Cyclotron Laboratory, Michigan State University, East Lansing, Michigan 48823
(Received 30 December 1971)

Inelastic proton scattering from ^{40}Ca has been measured at beam energies of 24.93, 30.04, 34.78, 34.78, and 39.83 MeV. Angular distributions from 13 to 97° for about 40 inelastic states were obtained. Analyses with both microscopic and macroscopic theories are presented.

I. INTRODUCTION

The double magic nuclei, such as ^{40}Ca, have been studied in great detail both experimentally and theoretically. The degree of deviation from a simple double-closed-shell structure is of great interest. Recent advances in the theories of nuclear shell models [random-phase approximation (RPA) and deformed], the effective nucleon-nucleon force, and the distorted-wave treatment of direct reaction enable one to formulate a microscopic description of the inelastic scattering of protons by nuclei.[1-6] The ^{40}Ca nucleus was chosen as a target to test the (p, p') reaction as a probe of nuclear structure because of the following points: First, it is a target which allows the (p, p') reaction to examine all the components of the proton-nucleus force. Second, it is a target in which the eigenvectors describing the excited states are relatively well established both experimentally and theoretically. Third, it is a target for which good optical-model parameters exist.

The structure of ^{40}Ca has also been investigated in other experiments such as (α, α'),[7,8] (e, e'),[9,10] $(^3He, d)$,[11] (d, n),[12] and $(p, p'\gamma)$.[13] The (α, α') reaction is a predominantly surface-dominated reaction and it leads to diffraction scattering. It measures L transfer for the excited normal-parity states, and the isoscalar component of the projectile-nucleon force. The (e, e') reaction gives reduced electromagnetic transition probabilities and multipolarities. The $(^3He, d)$ and (d, n) proton stripping reactions allow one to study individual components of the vectors of the excited states. The $(p, p'\gamma)$ reactions have been used primarily to determine the spins and parities of the excited states; whereas, the (p, p') reaction is useful in probing various components of the effective interaction and testing microscopic wave function.

By studying the energy dependence of the reaction, in many cases, one is able to remove ambiguities due to reaction mechanism problems. The present experiment studies proton inelastic scattering from ^{40}Ca at bombarding energies of 24.93, 30.04, 34.78, and 39.83 MeV. Spectra were taken simultaneously by two surface-barrier Ge(Li) detectors with an over-all resolution of 30 keV [full width at half maximum (FWHM)]. Angular distributions for inelastic scattering to approximately 50 excited states were obtained over the angular range from 13 to 97° (lab). The data were analyzed using both a collective model to extract L transfers and nuclear deformations and a microscopic model employing a realistic force, RPA wave functions, and approximate exchange.

II. EXPERIMENTAL APPARATUS AND PROCEDURES

The data were obtained using protons from the Michigan State University sector-focused cyclotron.[14-16] The beam was energy-analyzed using two 45° bending magnets with image and object slits set to pass beam with fractional energy spread of $\pm 1.25 \times 10^{-4}$. Detailed discussions of the optical properties of the beam and of the energy-analysis system are given elsewhere.[17-19] The absolute energies of the proton beams were obtained from nuclear-magnetic-resonance calibrations of the magnets. The uncertainty in this absolute scale was ±0.1%.[17] The absolute beam energies for this experiment were 24.93 ± 0.03, 30.04 ± 0.03, 34.78 ± 0.04, and 39.83 ± 0.04 MeV.

The beam on the target was monitored using both a Faraday cup and a Ge(Li) proton detector placed at 45° with respect to the beam. The scattering chamber[20] used in this experiment consisted of a target chamber which was viewed through ports in a sliding seal. Two ports separated by 14.7° were coupled such that a pair of Ge(Li) proton detectors could be used. The solid angles of the two detectors were $1.38 \pm 0.04 \times 10^{-4}$ and $0.786 \pm 0.024 \times 10^{-4}$ sr for detectors 1 and 2, respectively. The angular range of detection was from 12 to 97° in 5° steps. Data were taken twice at 27 and 72° by each detector for the relative normalization. Details concerning these detectors are given in a previous publication.[21] The target was a rolled, self-supported 2-mg/cm²

TABLE I. Isotopic analysis of ^{40}Ca target used.

	Isotopic analysis (at.%)
^{40}Ca	99.973
^{42}Ca	0.008
^{43}Ca	0.001
^{44}Ca	0.018
^{46}Ca	<0.001
^{48}Ca	0.001

foil of enriched (99.973%) ^{40}Ca. The isotopic and spectroscopic analysis supplied by Oak Ridge National Laboratory is listed in Table I.

Dead-time corrections were made for all spectra including those taken by the monitor counter. The dead times for most spectra were under 2%. For only a very few cases (5 out of 100) in which the detector was set at a small angle, were corrections found to exceed 5%, the largest being 12%.

Representative spectra are shown in Figs. 1 to 4. In the group of elastic peaks two small ones can be seen, one of which is from high-Z contaminants and the other was identified as ^{19}F. States up to 10.3-MeV excitation energy were observed. The broad peak at high excitation energy was due to a tantalum degrader slit used as a collimator in front of the Ge(Li) detector. The ground state of the ^{40}Ca(p, d) reaction having a Q value of −13.863 MeV was also observed.

The over-all resolution was about 30 keV (FWHM). The sources and their contributions to the energy resolution are tabulated in Table II for 40-MeV protons.

TABLE II. Contributions to the energy resolution (40-MeV protons).

Sources	ΔE (keV)
Straggling	
Target	10.0
Package windows	5.3
Detector windows	8.0
Total	23.3
Electronic	7.2
Ion pair statistics	7.3
Beam spread	10.0
Kinematic (at 45°)	7.5
Over all	28.3

Angle Calibration

The laboratory angle for each spectrum was determined by the energy separations between the elastic peaks of ^{40}Ca, ^{16}O, and ^{12}C and the 3$^-$ excited state of ^{40}Ca at 3.736 MeV. The experimental energies of these peaks were calculated from the positions of their centroids. With the known energy difference between the ^{40}Ca (0.000 MeV) and the ^{40}Ca* (3.736 MeV) states at a particular angle, the energy spacing between these four peaks was computed. However, without knowing the exact angle, the energy calculation is only approximate. It was necessary to reiterate this angle and energy calibration procedure. Most computations required only two iterations since the energy difference between the ^{40}Ca* (3.736 MeV) and ^{40}Ca (0.000 MeV) states changes slowly with respect to angle (about 0.8 keV/deg at 25° and 1.7 keV/deg at 100°).

For laboratory angles less than 28°, the H(p, p)-H reaction was also used. The fact that the kinematics of this reaction is strongly dependent on angle provided an acute test of the accuracy of the method described above. The agreement between these two calibration methods was within 0.04°.

The effect of the uncertainties in the beam energy and in the centroids of peaks upon the accuracy of determinations of the laboratory angle was studied. Two kinematics calculations were done using $E_p = 35.000$ and 34.775 MeV. The laboratory angles calibrated by these two calculations agreed to within 0.1°. When the centroids were allowed to fluctuate ±0.2%, the calibrated angles varied by ±0.04°. We conclude that our angle calibration error is less than ±0.05°.

TABLE III. Absolute cross-section measurement comparison.

Target	E_p	$\theta_{c.m.}$ (deg)	Present experiment $(d\sigma/d\Omega) \pm \Delta$ [a] (mb) ± (%)	$(d\sigma/d\Omega) \pm \Delta$ (mb) ± (%)	Absolute error (%)	Reference
^{12}C	40	60	10.6 ± 2.4	10.3 ± 2.0	5.0	23
^{16}O	40	50	20.2 ± 2.0	20.2 ± 1	1.7	24
^{40}Ca	40	41	96.2 ± 0.2	96.7 ± 2.0	5.0	23
^{40}Ca	30	46	109.6 ± 0.2	110.1 ± 1.7	3.0	25

[a] Statistical error only.

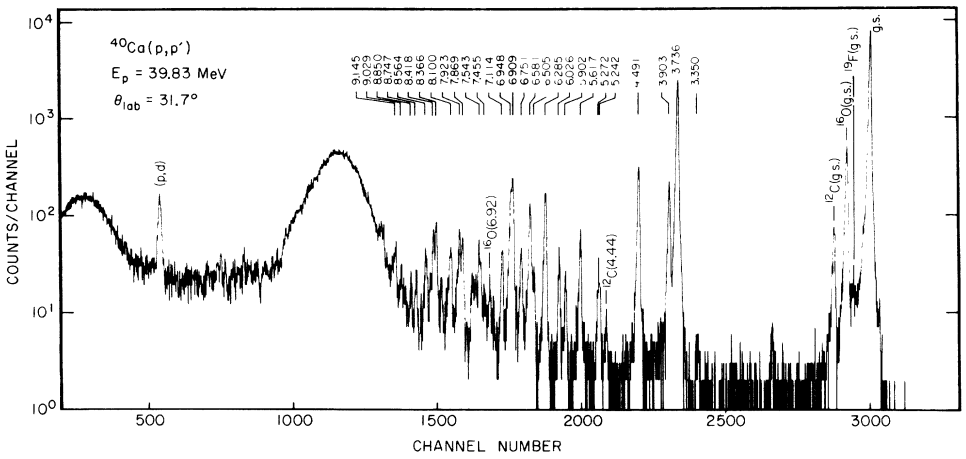

FIG. 1. ^{40}Ca(p, p')^{40}Ca* spectrum taken at $\theta_{lab} = 31.7°$ for $E_p = 39.83$ MeV.

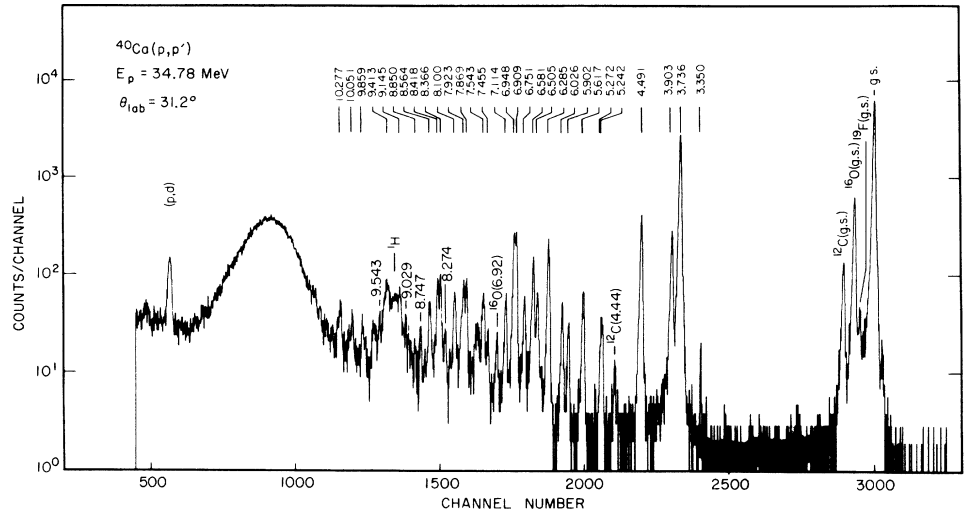

FIG. 2. ^{40}Ca(p, p')^{40}Ca* spectrum taken at $\theta_{lab} = 31.2°$ for $E_p = 34.78$ MeV.

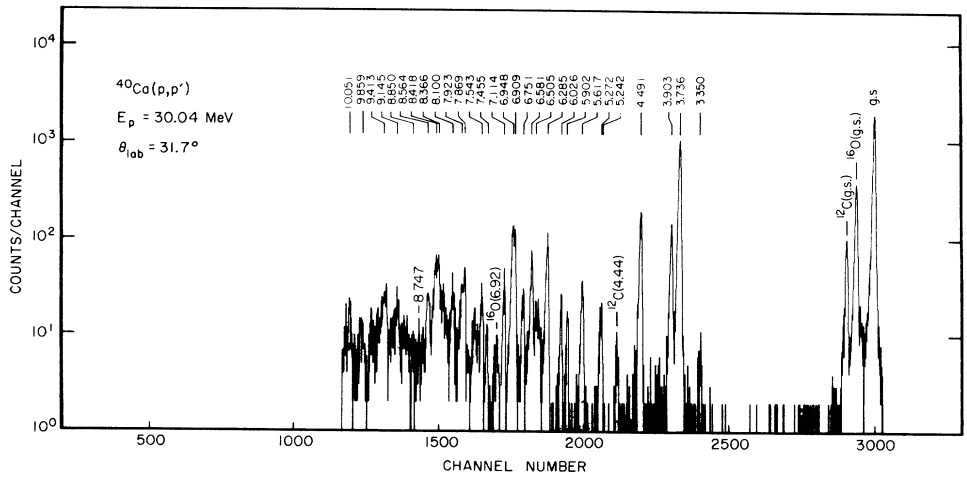

FIG. 3. ^{40}Ca(p, p')^{40}Ca* spectrum taken at $\theta_{lab} = 31.7°$ for $E_p = 30.04$ MeV.

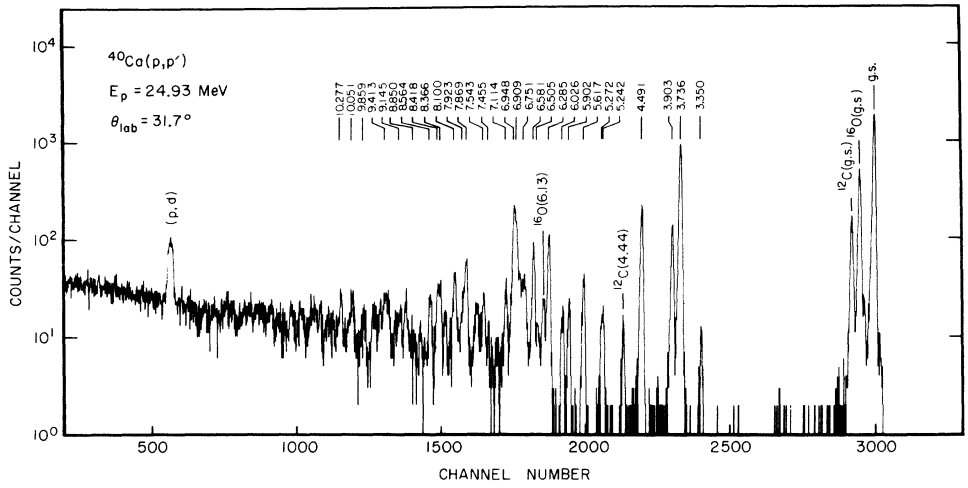

FIG. 4. ^{40}Ca$(p, p')^{40}$Ca* spectrum taken at $\theta_{lab} = 31.7°$ for $E_p = 24.93$ MeV.

Absolute Cross Sections

The detector, monitor, and Faraday-cup system were calibrated using proton scattering from the hydrogen contained in a clear Mylar target. The cross section for this reaction is known to ±0.5% at these energies.[22] As a check of this calibration procedure, differential cross sections were measured for elastic proton scattering from ^{12}C, ^{16}O, and ^{40}Ca. A comparison of these measurements with those of other references[23-25] is given in Table III. The errors given for this experiment in Table III are statistical only.

A detector efficiency of 0.9875[26] was assumed for these measurements. If one uses these additional measurements as a part of the cross-section calibration, an error of ±3% can be assigned to our cross-section measurements.

Treatment of Data from Contaminant Nuclei

The main contaminants observed were ^{1}H, ^{12}C, and ^{16}O. The hydrogen and carbon came from the

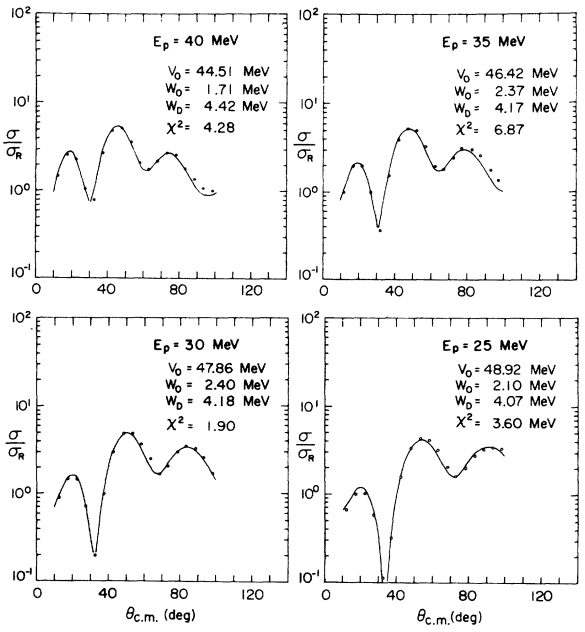

FIG. 5. Optical-model fits to the experimental elastic scattering results at $E_p = 25$ to 40 MeV.

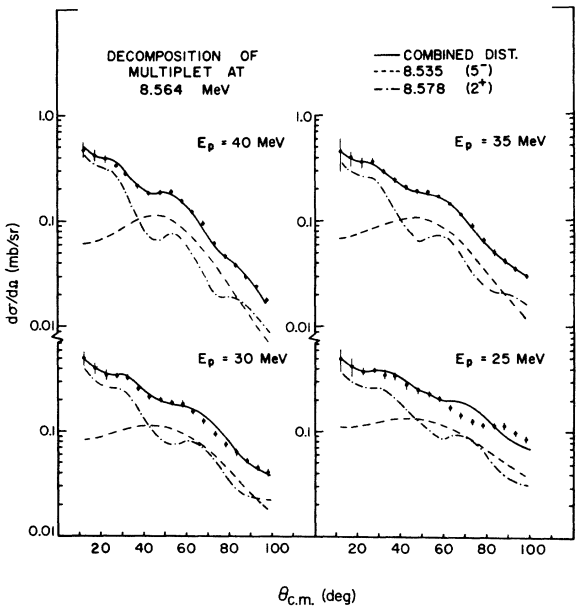

FIG. 6. The decomposition of doublet at $E_x = 8.558$ MeV.

deposition of pumping oil on the target, while the oxygen came from the oxidation of the Ca during the mounting of the target foil. The contamination of spectra due to peaks in the response function of Ge(Li) detector is ruled out by inspection of the spectra.

A complete analysis was made for ^{12}C and ^{16}O states. A Mylar target was used to measure the ratio of counts of the inelastic to the elastic peaks at the identical angles at which ^{40}Ca data were taken. This method provided a reference to monitor the intensity of the contaminant peaks in the ^{40}Ca spectra. Once the ratio of counts in the Mylar run was computed, the number of counts for the same inelastic contaminant peak in a ^{40}Ca spectrum was easily determined as long as the elastic counts were known.

The corrections for contaminants at small angles, where the ^{12}C and ^{16}O elastic peaks could not be separated from that of ^{40}Ca, required a measurement of the amount of each contaminant in the target. The angular distribution of relative cross sections in the laboratory system for the ^{16}O elastic peak was first obtained. This result was compared with the measurement reported by Cameron.[24] Good agreement in the shape of the distribution was noted. This suggested that the amount of ^{16}O on the target remained essentially constant in the course of the whole experiment. Secondly, the amount of ^{16}O in the target was calculated by using Cameron's data. Several values were computed over a few angles around $\theta_{lab} = 50°$ where the distribution is flat. The average value of the amount of ^{16}O in the ^{40}Ca target used was found to be 0.0192 ± 0.002 mg/cm^2. Similarly, the thickness of ^{12}C was measured to be 0.00258 ± 0.0003 mg/cm^2. This method allowed a correction at each energy to be made to that data in which the contaminant was not resolved from the state in ^{40}Ca.

The angular distributions of the differential cross sections for elastic scattering in the center-of-mass system are shown in Fig. 5.

Decomposition of Multiplets

On the basis of Grace and Poletti's spectrum,[27] we know that several pairs of doublets with $\leq$20-keV separation were seen as single peaks in our spectra. Individual distributions could not be extracted directly from spectra for these states. It was decided that the angular distribution for the composite peak be analyzed first. Then, decomposition was done whenever it was possible.

Figure 6 illustrates the decomposition of the doublet at 8.564 MeV. The L transfers to the component states were tentatively determined by examining the over-all shape of the combined distribution. In this case they are $L = 5$ and $L = 2$. The shapes of the experimental angular distributions of the 4.917 (5^-) and the 3.903 (2^+) states were used in the decomposition and the ratio of cross sections was obtained by finding the best fit to all distributions at four energies. These fits are shown in Fig. 6.

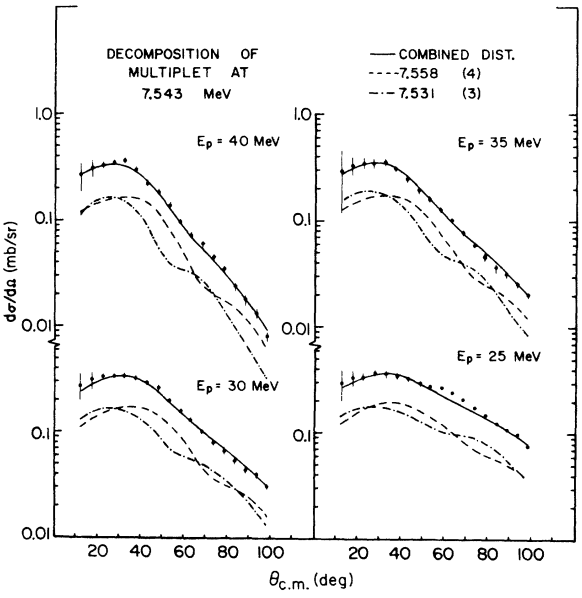

FIG. 7. The decomposition of doublet at $E_x = 7.539$ MeV.

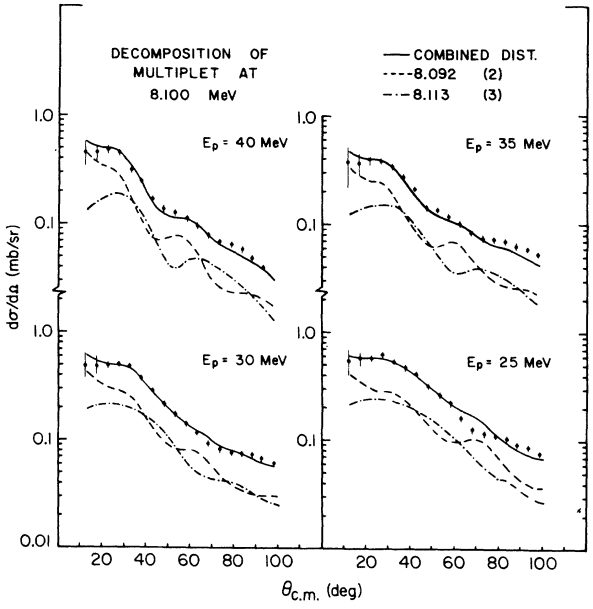

FIG. 8. The decomposition of doublet at $E_x = 8.097$ MeV.

In addition to the criterion of being a good fit for all four beam energies, the difference in differential cross section at various angles must also be consistent with the change of peak shape and centroid from one spectrum to another. It was found that the change of peak shape for this multiplet agreed with the above analysis. This also provided a way to determine the association of the spin and the excitation energy of the component states. The differential cross sections so obtained are estimated to be accurate to 30%.

Similar analyses were applied to the doublets at 7.543 and 8.100 MeV. The results are shown in Figs. 7 and 8. For the composite peak at 7.543 MeV, a fit was obtained by using the experimental distributions from the 3^- (3.736 MeV) and the 4^+ (6.505 MeV) states. Because of the similarity of $L=3$ and $L=4$ angular distributions, this assignment of spins is considered to be highly questionable.

The components of the 8.100-MeV doublet were assigned $L=2$ and $L=3$. It should be noted that the experimental angular distribution for the 6.285-MeV state, instead of that for the 3.733-MeV state, was used for the $L=3$ distribution to obtain the best over-all fit.

Grace and Poletti observed a triplet with excitation energies at 6.909, 6.930, and 6.948 MeV. The 6.930-MeV level was seen to be the strongest among this triplet in their spectrum taken at 87.5° at $E_p = 13.065$ MeV. As shown in Fig. 9, the first and third members of this triplet were quite well resolved at smaller angles while the middle one was not seen. The solid line is drawn using a well

TABLE IV. Excitation energy measurements, ^{40}Ca. Energies in keV.

$E_p = 25$ MeV $E^* \pm \Delta E$		$E_p = 30$ MeV $E^* \pm \Delta E$		$E_p = 35$ MeV $E^* \pm \Delta E$		$E_p = 40$ MeV $E^* \pm \Delta E$		All energies $E^* \pm \Delta E$	
3736	1	3736	1	3736	1	3736	1	3736	1
3903	1	3902	1	3904	1	3904	1	3903	1
4490	2	4491	1	4491	1	4491	1	4491	1
5261	7	5261	5	5256	5	5264	5	5263	6
5617	3	5618	2	5617	4	5618	4	5617	3
5901	5	5904	1	5904	2	5901	5	5902	4
6026	3	6026	3	6027	2	6026	3	6026	3
6286	1	6284	2	6285	1	6285	1	6285	1
6499	6	6505	5	6510	4	6508	3	6505	6
6580	2	6582	2	6582	3	6582	2	6581	2
6750	4	6752	2	6751	4	6752	5	6751	4
6929	4	6927	6	6924	5	6923	3	6926	5
7114	1	7115	2	7113	1	7114	1	7114	1
7455	3	7453	5	7456	4	7458	6	7455	5
7540	5	7542	5	7545	1	7546	3	7543	5
7671	8	7676	9	7672	1	7673	7	7673	8
7867	4	7868	5	7871	1	7871	2	7869	4
7919	6	7923	4	7924	2	7927	5	7923	6
8097	6	8100	5	8102	3	8100	3	8100	5
8360	7	8366	3	8370	2	8368	5	8366	6
8416	6	8419	4	8420	4	8419	3	8418	4
8563	5	8565	5	8566	4	8564	7	8564	6
8741	7	8750	3	8749	2	8748	5	8747	6
8849	6	8851	3	8849	3	8849	4	8850	4
				8978	6			8978	6
				9029	5			9029	5
				9145	5			9145	5
				9237	3			9237	3
				9360	5			9360	5
				9413	5			9413	5
				9591	4			9591	4
				9642	6			9642	6
				9859	4			9859	4
				10051	3			10051	3
				10277	3			10277	3

resolved peak to give a representative "standard" singlet peak.

At laboratory angles equal to 12 and 27°, the quality of fit and the cleanness in the valley suggested that the differential cross section of the middle level at 40-MeV beam energy is less than 0.02 mb/sr in this angle range. Hence the differential cross sections for the 6.909 and 6.948 states are believed to be fairly accurate, and the spin assignments for these two states can be made more or less unambiguously. At larger angles good fits were still achieved, although the middle level started to show up. The angular distributions for the 6.909 and 6.948 states are discussed in the following sections.

Calibration of Excitation Energies

The excitation energies of the observed levels of ^{40}Ca have been measured in previous works (see Sec. V). Below 9 MeV, every state seen in this experiment was also reported by Grace and Poletti. However, it was decided to carry out the energy calibration to check the linearity of the data-accumulation system used in this work and to determine the excitation energies of those states which lie above 9 MeV.

The calibration energies for reference peaks were 3.7368 (3$^-$), 4.4917 (5$^-$), and 6.2850 MeV (3$^-$) taken from Poletti *et al.*[28] and the 7.1133 state from Dolan and McDaniels.[29] The results of the calculation are listed in Table IV. The energy shown for a given peak was obtained by averaging over the results from most of the spectra at each beam energy and again over all four energies. As can be seen in the table, the consistency of the experimentally determined excitation energy for every state was within ±10 keV. Comparisons with other experiments are discussed in Sec. V. No attempt was made to calibrate the energies for closely spaced multiplets.

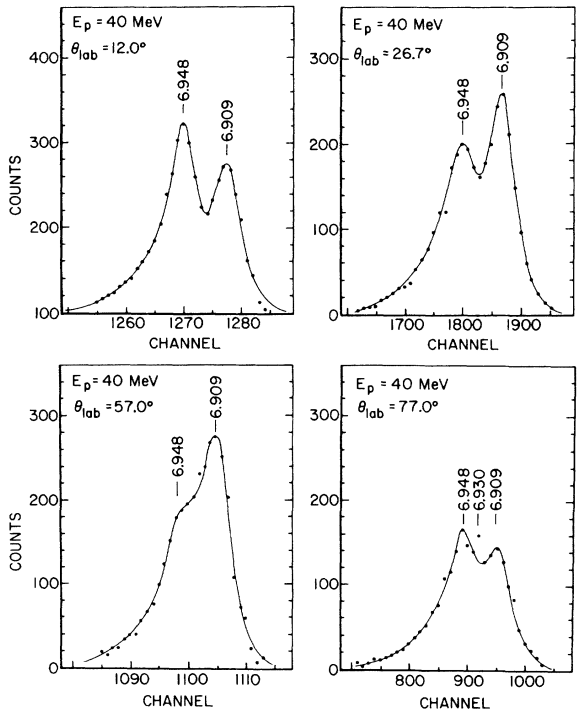

FIG. 9. Spectrum fits using two superimposed standard peaks for the analysis of 6.909, 6.930, 6.948 triplet.

III. DWBA AND COLLECTIVE-MODEL ANALYSIS

The theory and use of the distorted-wave born approximation (DWBA) and the collective model to analyze inelastic proton scattering have been presented extensively elsewhere.[30-32] In particular, we will use the procedures and terminology set forth in Ref. 30.

Elastic Scattering

In order to obtain parameters for the distorted waves used in the DWBA calculations, the angular distributions of elastic scattering were analyzed for each energy using a standard optical potential (c.f. the work of Fricke *et al.*[33])

The geometrical parameters (r_0 and a) for the various terms in the optical potential and the average spin-orbit strength (V_{so}) were taken from the analysis of elastic scattering and polarization measurements for 40-MeV protons on 11 nuclei from ^{12}C to ^{208}Pb.[33] The remaining parameters, V_0, W_0, and W_D, were varied to give the best fit to the data. The results are listed in Table V. These parameters were used for all the DWBA calculations presented in this study.

The elastic data, in ratio to Rutherford scattering, and the final optical-model calculation are shown in Fig. 5.

TABLE V. Optical parameters:

r_R = 1.16 F,	a_R = 0.75 F
r_I = 1.37 F,	a_I = 0.63 F
r_{so} = 1.064 F	a_{so} = 0.738 F
V_{so} = 6.04 MeV	r_C = 1.25 F

E_p (MeV)	V_0 (MeV)	W_0 (MeV)	W_D (MeV)	χ^2
25	48.92	2.10	4.07	3.60
30	47.86	2.40	4.18	1.90
35	46.42	2.37	4.17	6.87
40	44.51	1.71	4.42	4.28

DWBA Calculations

The distorted-wave calculations were made using a FORTRAN-IV version of the Oak Ridge computer code JULIE[34] implemented to run on the Michigan State University Cyclotron Laboratory XDS Sigma-7 computer. The input consists of three major parts corresponding to the elements in the integral of the transition amplitude, i.e., the form factor, the entrance-channel wave function (incoming distorted wave), and the exit channel (outgoing distorted wave). The form factors used for the collective model deformed both the real and imaginary parts of the optical potential. Coulomb excitation was included for L transfers of 2 and 3 in the collective-model analysis. Spin-flip contributions were not included.

The entrance channel was described by the optical-model parameters listed in Table V. The optical parameters for the exit channel depend on whether the Q value was considered or not. Figure 10 summarizes the general results of the calculations for $L=2$ and $L=8$ and for energy dependence, as well as the Q-value effect. For $L=8$, a spin-orbit term in the optical potential can not be included unless $j=L$ (Table I, Ref. 34). In order to estimate the effect of the spin-orbit potential on the distribution, calculations were made with and without this term in both entrance and exit channels for the case of $L=6$. It was found that the effect is small except for 25 MeV as illustrated.

The deformation parameters, β_L, were obtained by calculating the ratio of the cross sections $\sigma(\text{exp})$ and $\sigma_L(\text{JULIE})$, each integrated over the angular range of this experiment. The deformation, δ_L, is defined as $B_L R_0$, where R_0 is the real

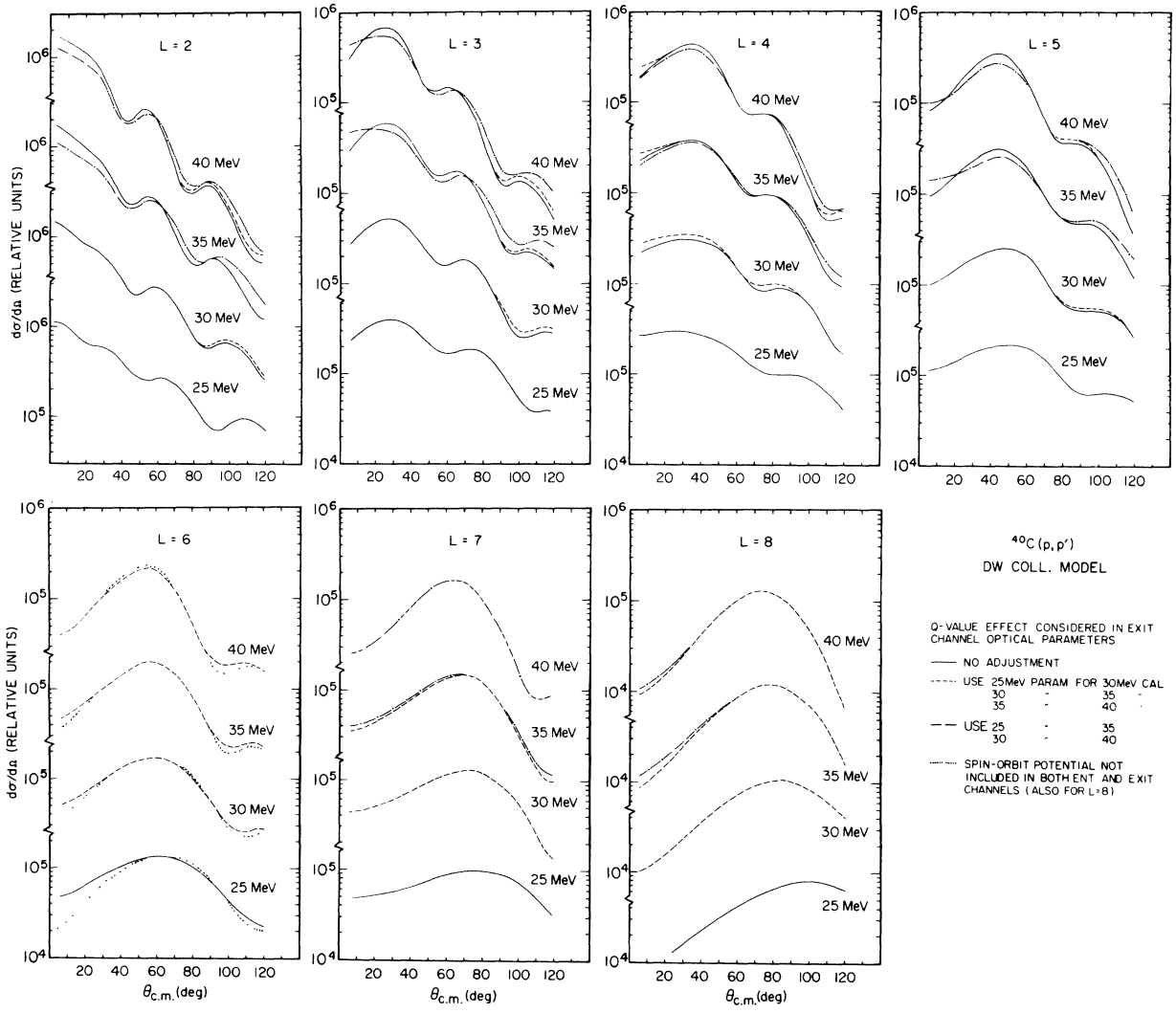

FIG. 10. Summary of the DWBA calculations using collective-model form factor for $L=2$ to $L=8$ at $E_p=25$ to 40 MeV.

radius of the target nucleus. $R_0 = 3.96$ F was used for all the calculations.

The experimental angular distributions of the states at 3.903 (2^+), 3.736 (3^-), 6.285 (3^-), 6.505 (4^+), and 4.491 MeV (5^-) were used as empirical standards to assist in the determination of the L transfers to other states. It was found that most of the angular distributions with the same L at the same bombarding energy resemble each other in shape. Distributions revealing possible differences in microscopic structure and reaction mechanism were also noted. Since there are four distributions from four bombarding energies for each state which could be compared with the standards, the ambiguities in determining the L transfer for a given state were minimized.

The L assignments to the components of a doublet were obtained from a decomposition method (see Sec. II). The high-spin states having $L = 6$ or $L = 7$ were identified by fitting the data to the DWBA angular distributions.

Distorted-wave collective-model calculations were done for every state with appropriate adjustments for the Q value in exit channels. Nuclear

TABLE VI. Deformations as a function of beam energy for ^{40}Ca.

		δ_L (F)			
E^* (keV)	L	$E_p = 24.93$ MeV	$E_p = 30.04$ MeV	$E_p = 34.78$ MeV	$E_p = 39.83$ MeV
3736	3	1.40	1.38	1.35	1.32
3903	2	0.42	0.43	0.42	0.43
4491	5	0.91	0.86	0.83	0.80
5249	2	0.15	0.14	0.12	0.12
5279	4	0.16	0.15	0.14	0.13
5617	5	0.42	0.36	0.33	0.31
6026	3	0.23	0.20	0.18	0.17
6285	3	0.46	0.43	0.41	0.40
6505	4	0.18	0.17	0.18	0.17
6581	3	0.41	0.36	0.33	0.32
6751	3	0.27	0.24	0.22	0.21
6909	2	0.44	0.43	0.42	0.45
7114	5	0.40	0.32	0.29	0.27
7292	2	0.10	0.10	0.09	0.09
7455	4	0.20	0.17	0.16	0.15
7531	3	0.19	0.17	0.17	0.15
7558	4	0.23	0.20	0.20	0.19
7869	2	0.28	0.25	0.23	0.23
7923	4	0.34	0.31	0.29	0.29
8092	2	0.18	0.17	0.17	0.16
8113	3	0.19	0.17	0.16	0.15
8191	6	0.22		0.15	
8366	4	0.32	0.31	0.31	0.33
8418	3	0.29	0.27	0.25	0.25
8535	5	0.23	0.20	0.19	0.18
8578	2	0.18	0.17	0.17	0.17
8747	2	0.17	0.15	0.15	0.14
8850	7	0.10	0.10	0.09	0.09
8978	6			0.17	0.15
9029	5			0.16	0.15
9145	3			0.23	
9237	7			0.06	
9360	3			0.16	
9413	3			0.26	
9541	4			0.15	
9591	3			0.12	
9859	5			0.19	
10051	5			0.19	
10277	4			0.18	

TABLE VII. Reduced transition probabilities in single-particle Weisskopf units, "mass-transport" parameters, and "force constants" for ^{40}Ca.

E^* (keV)	L	G_{sp}	$B_L/\hbar^2$ (MeV)$^{-1}$	C_L (MeV)	E^* (keV)	L	G_{sp}	$B_L/\hbar^2$ (MeV)$^{-1}$	C_L (MeV)
3736	3	26.6	0.11 2	0.15 3	8113	3	0.4	0.36 3	0.24 5
3903	2	2.1	0.74 2	0.11 4	8191	6	0.7	0.77 3	0.52 5
4491	5	17.2	0.37 2	0.75 3	8366	4	1.9	0.11 3	0.80 4
5249	2	0.2	0.70 3	0.19 5	8418	3	0.9	0.14 3	0.98 4
5279	4	0.4	0.97 3	0.27 5	8535	5	0.9	0.39 3	0.28 5
5617	5	2.6	0.19 3	0.61 4	8578	2	0.3	0.22 3	0.16 5
6026	3	0.5	0.36 3	0.13 5	8747	2	0.3	0.27 3	0.21 5
6285	3	2.4	0.69 2	0.27 4	8850	7	0.4	0.21 4	0.17 6
6505	4	0.6	0.45 3	0.19 5	8978	6	1.0	0.52 3	0.42 5
6581	3	1.6	0.99 2	0.43 4	9029	5	0.6	0.51 3	0.41 5
6751	3	0.7	0.22 3	0.99 4	9145	3	0.8	0.15 3	0.12 5
6909	2	2.1	0.44 2	0.20 4	9237	7	0.2	0.48 4	0.41 6
7114	5	2.0	0.20 3	0.99 4	9360	3	0.4	0.29 3	0.26 5
7292	2	0.1	0.86 3	0.46 5	9413	3	1.0	0.12 3	0.10 5
7455	4	0.5	0.50 3	0.28 5	9541	4	0.4	0.43 3	0.40 5
7531	3	0.4	0.35 3	0.20 5	9591	3	0.2	0.50 3	0.46 5
7558	4	0.8	0.31 3	0.18 5	9859	5	0.9	0.32 3	0.31 5
7869	2	0.6	0.13 3	0.80 4	10051	5	0.9	0.30 3	0.30 5
7923	4	1.6	0.14 3	0.88 4	10277	4	0.6	0.27 3	0.29 5
8092	2	0.3	0.23 3	0.15 5					

TABLE VIII. Fraction of sum rules exhausted for ^{40}Ca at 35 MeV.

E^* (keV)	L	Energy weighted sum rule	Non-energy-weighted sum rule	E^* (keV)	L	Energy weighted sum rule	Non-energy-weighted sum rule
3736	3	0.221	0.538	8113	3	0.007	0.007
3903	2	0.032	0.058	8191	6	0.008	0.006
4491	5	0.064	0.187	8366	4	0.021	0.028
5249	2	0.003	0.005	8418	3	0.017	0.018
5279	4	0.002	0.005	8535	5	0.006	0.009
5617	5	0.012	0.029	8578	2	0.011	0.009
6026	3	0.007	0.010	8747	2	0.009	0.007
6285	3	0.034	0.049	8850	7	0.001	0.002
6505	4	0.005	0.009	8978	6	0.005	0.008
6581	3	0.024	0.033	9029	5	0.005	0.007
6751	3	0.011	0.015	9145	3	0.016	0.016
6909	2	0.057	0.058	9237	7	0.001	0.001
7114	5	0.012	0.022	9360	3	0.008	0.008
7292	2	0.003	0.003	9413	3	0.020	0.020
7455	4	0.005	0.007	9541	4	0.005	0.006
7531	3	0.007	0.008	9591	3	0.005	0.004
7558	4	0.008	0.011	9859	5	0.007	0.010
7869	2	0.018	0.017	10051	5	0.008	0.010
7923	4	0.017	0.024	10277	4	0.009	0.009
8092	2	0.010	0.009				

deformations were then extracted. The assigned L values and the deformation parameters along with other physical quantities are listed in Tables VI to IX. The experimental data, the collective-model fits, and the standard distributions are shown in Figs. 11 to 15, where the solid curves are collective-model calculations and dashed curves show the shapes of the standard distributions.

The main features of the data presented in Figs. 11 to 15 are as follows:

(1) The structure of the angular distributions becomes more pronounced as the beam energy increases, thus enabling an L-transfer assignment to be most easily achieved at the higher energy.

(2) The fractional deformation parameter, δ_L, is seen to be independent of energy (over this limited energy range and within the experimental uncertainties of the data).

Figure 16 shows the experimental cross sections obtained for three $L = 1$ states at 5.092, 6.948, and 8.274 MeV. The solid curves drawn against the data of 5.902 MeV are the results of collective-model calculations. It is seen that the fits are very poor, therefore deformation parameters were not obtained for $L = 1$ states. A possible explanation of this result is that under the imcompressibility constraint, the $L = 1$ vibration corresponds to the oscillation of the center of mass of the nucleus, which, of course, is not the excitation observed. A microscopic description which accounts for the first and second 1^- states is given in a later section of this paper.

The collective model using only the radial vibration also failed to reproduce the shapes of the distributions for the 0^+ first excited state (3.350

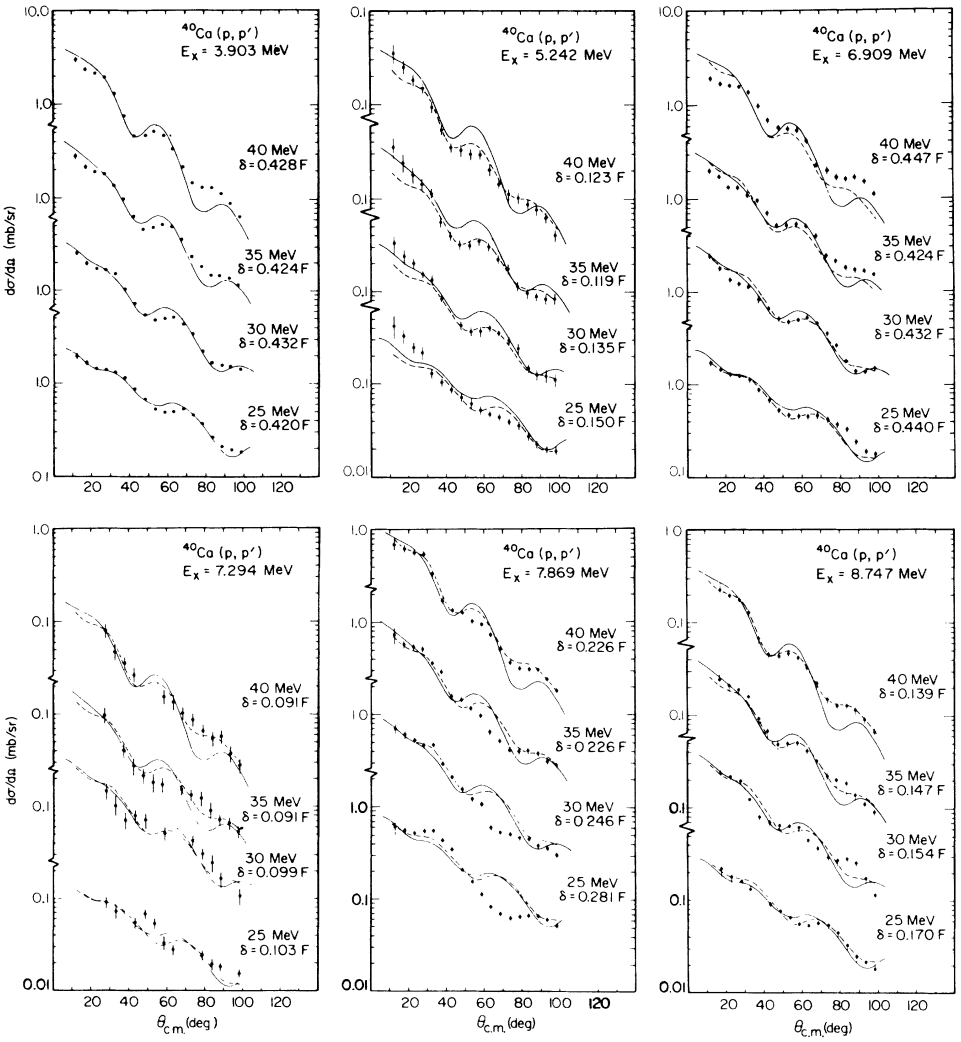

FIG. 11. Experimental distributions of $L = 2$ states and collective model fits (solid curves). The dashed curves are those of 3.903-MeV state.

MeV). Calculations for this state based on a generalized collective vibrational model have been carried out by Satchler[35,31] at 25 MeV but no data were available at the time those calculations were made. In this generalized model, the potential $U(V, R, a, r)$ can be deformed with respect to any or all of its parameters with the constraint that the volume integral remain constant. This leads to an interaction of the form

$$\delta U = \delta R \frac{\partial U}{\partial R} + \delta V \frac{\partial U}{\partial V} + \delta a \frac{\partial U}{\partial a}.$$

DWBA calculations were made at all four bombarding energies using each of these terms and various combinations of them. Some of these calculations at 25 MeV are shown in Fig. 17. The breathing mode is the usual radial vibration ($\delta a = \delta V = 0$) and the "a-vibration" calculations allow for δV and δR to be zero. The normalization of the curves to the data will allow the normalization, β_0^2, to be determined. It is seen that the curves bear very little resemblance to the data. Similar disagreement exists at 30, 35, and 40 MeV. We also made calculations in which the parameters, V, R, and a were varied on a gridlike basis and calculations which used complex interactions within the framework of this theory. No fit was found.

We next assumed the empirical form factor of the form:

$$F(r) = e^{-(r-R+a)^2/a} - B\, e^{-(r-R+a)^2/a}.$$

The choice of this form factor was made such that a node would appear in the nuclear-surface region. After searching on R, a, and B, it was found that the data could be fitted qualitatively using the form factor shown in Fig. 18. A comparison between

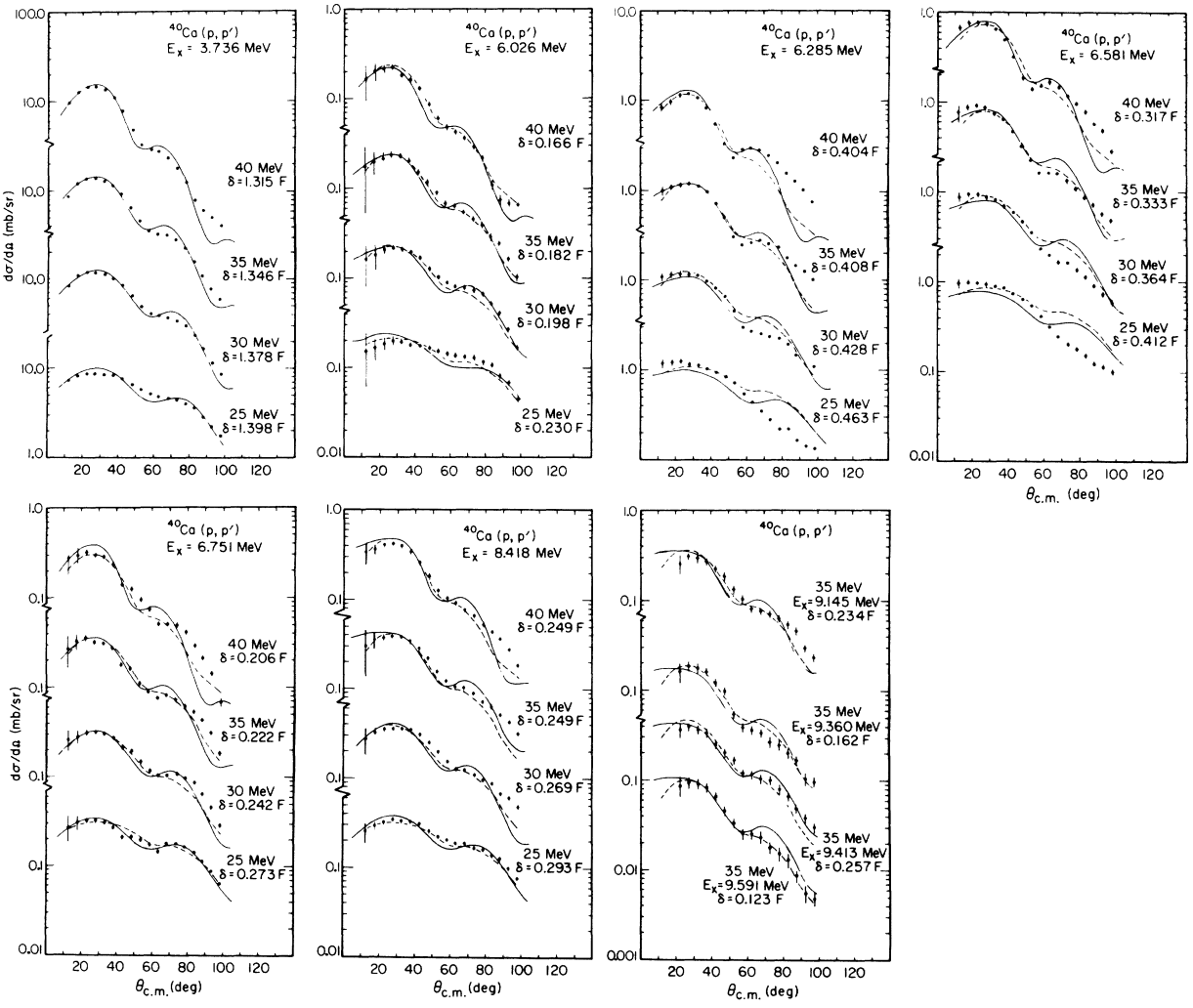

FIG. 12. Experimental distribution of $L = 3$ states and collective-model fits (solid curves). The dashed curves are those of 3.736-MeV state.

the data and the calculated cross sections using this form factor is also shown in Fig. 18. The main difference between this form factor and that of the a-vibration form factor is in the relative size of the oscillation at the surface. However, if one postulates that the ground state and the excited 0^+ state are mixed spherical and deformed, as has been suggested,[36,37] then one may expect a form factor similar to the empirical form factor.[31] This and other microscopic considerations for this state will be discussed in Sec. V.

The values of δ_L for ^{40}Ca(p,p') are listed in Table VI for the bombarding energies 24.93, 30.04, 34.78, and 39.83 MeV along with the L-transfer assignment. These values of δ_L were used with Eq. (4) of Ref. 32 to find the reduced transition probabilities for the ground-to-excited-state transitions. In the approximation that the excitations are described in terms of harmonic vibrations, Eqs. (2) and (3) of Ref. 32 were used to calculate the "force constant," C_L, and "mass transport" parameters, B_L. The results of these calculations, along with a comparison of the reduced transition probability in single-particle units, G_{sp}, is given in Table VII. In Table VIII we list the fraction of the sum rules [Eqs. (5) and (6) of Ref. 32] exhausted for each transition.

IV. MICROSCOPIC DESCRIPTION

A great deal of work, both theoretical and experimental, has been directed towards the understanding of the energy level scheme and transition rates in ^{40}Ca in terms of the shell model and its

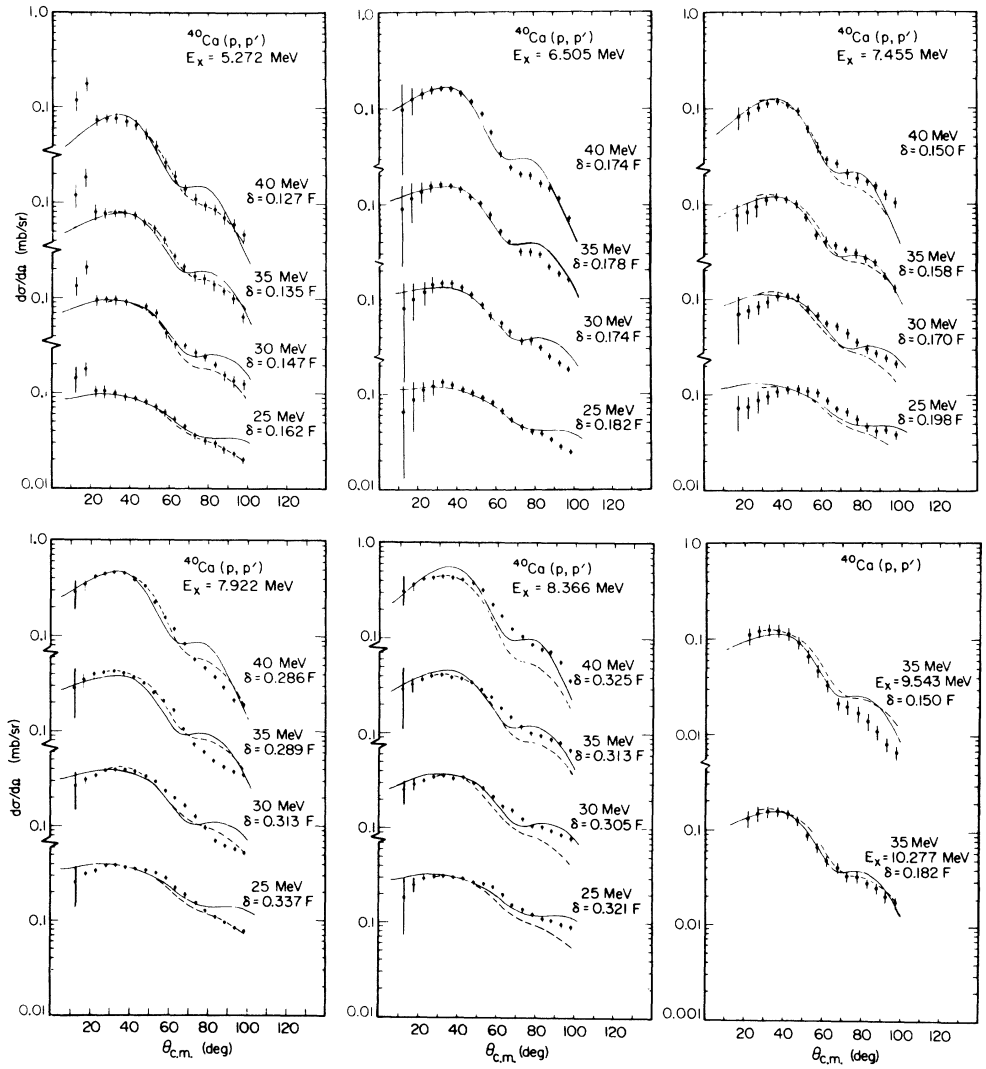

FIG. 13. Experimental distributions of $L=4$ states. Solid curves are collective-model fits. Dashed curves are those of 6.505 state.

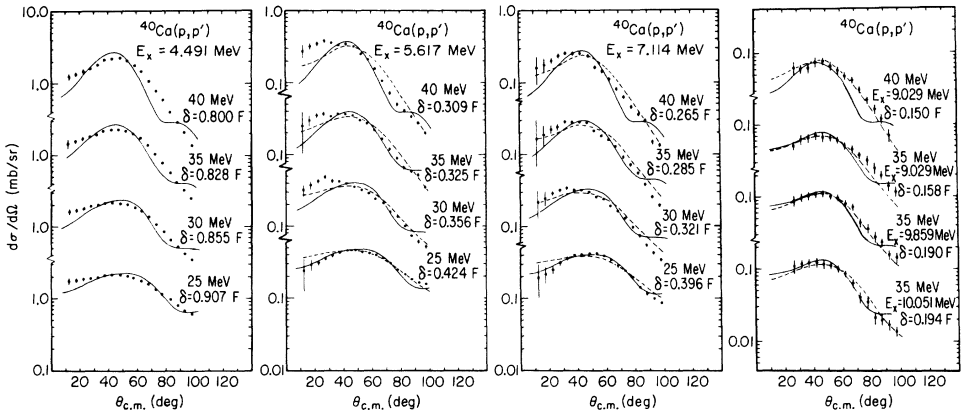

FIG. 14. Experimental distribution of $L=5$ states and collective-model fits (solid curves). The dashed curves are those of 4.491-MeV state.

extensions.[1-6] The properties of the negative-parity states in ^{40}Ca have been most vigorously investigated. The RPA seems to give a reasonably good description of the salient features of these states which are formed predominately, although not entirely, from single-particle–single-hole excitations. Positive-parity states are likely to contain large admixtures of many-particle–many-hole excitations, i.e., deformed components, and are not so easily described.

Recently, progress has been made in describing the (p,p') reaction in terms of a direct interaction between the projectile and target nucleons through an effective force. The properties of the effective force are largely dictated by the empirical two-nucleon potential. In particular, it has been shown by comparison with (p,p') data that the bound-state reaction matrix ("bare" effective force between bound nucleons) is a good guess at the "bare" effective force in the inelastic scattering process when the laboratory energy of the projectile is in the range from 15–70 MeV.[38-40] This conclusion is based on the studies of strong, normal-parity inelastic transitions and the real well of the optical potential which mainly test the strong central isoscalar component of the force. In these studies it was found that exchange effects are important, as was originally pointed out by Amos, Madsen, and McCarthy.[38]

In the present work, microscopic DWBA calculations are performed for some of the negative-pairty states of ^{40}Ca and comparisons made with our (p,p') data. RPA state vectors of Kuo[41] are used for the states of ^{40}Ca in the calculation and exchange effects are included approximately[40,42] in the DWBA calculations. For further discussion on this approximation see Love and Satchler.[43] In the following discussion, these calculations will be referred to as antisymmetrized distorted-wave (ADW) calculations. The Kallio-Kolltveit (KK) force and the central part of the Hamada-Johnston (HJ) force are used for the projectile-target in-

TABLE IX. Ratio of total cross sections $\sigma(D+E)/\sigma(D)$.

	3^-		5^-	
E_p (MeV)	Schaeffer (Ref. 39)	This work	Schaeffer (Ref. 39)	This work
17.3	2.7		6.8	
20.3	3.3		7.9	
25.0		3.5		7.8
30.0	2.9	3.1	6.4	6.4
35.0		2.8		5.5
40.0	2.5	2.5	4.6	4.8
50.0	2.3		3.6	

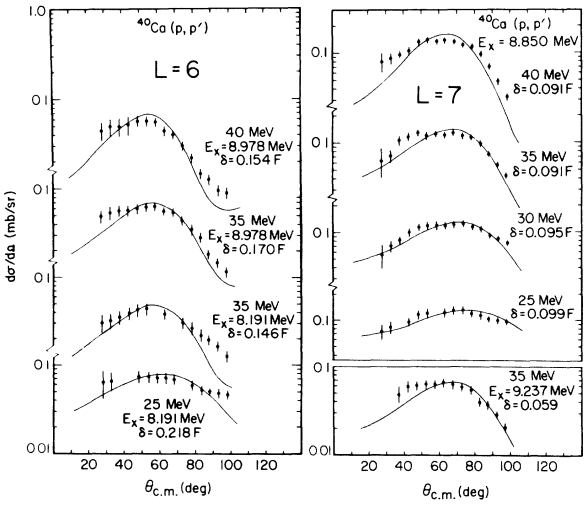

FIG. 15. Experimental distributions of $L=6$ and $L=7$ states, and collective-model fits (solid curves).

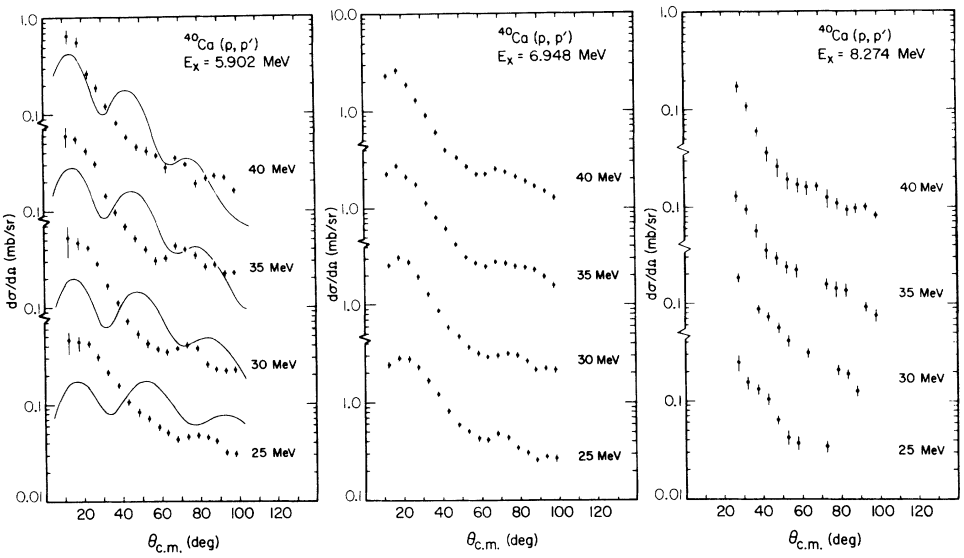

FIG. 16. Experimental distributions of $L=1$ states. The solid curves show the poor collective-model predictions.

teraction. The latter is basically the same force which has been used in the RPA calculation.

Wave Functions

Extensive calculations for the ground state and the odd-parity states of ^{40}Ca in terms of particle-hole configurations using the RPA method have been carried out by Gillet and Sanderson,[1,2] Kuo,[3] Leenhouts,[5] Dieperink, Leenhouts, and Brussaard,[6] and Perez.[44] Effects of spherical and deformed state mixing between the odd-parity states have also been reported by Gerace and Green.[4] In addition a simple shell-model picture for this nucleus was given by Erskine,[45] Seth *et al.*,[11] and Fuchs, Grabisch, and Roschert.[12]

The prediction of Gillet and Sanderson results from diagonalization of the matrix elements of the effective two-body force taken between the single-particle–single-hole shell-model states. The unperturbed energy of a particle-hole configuration is the appropriate value determined by experiments. The energies for proton particle-hole states are taken from those of ^{41}Sc and ^{39}K with $\Delta E(d_{3/2}^{-1}f_{7/2})$ equal to 6.71 MeV, and for neutron states the energies are from ^{41}Ca and ^{39}Ca with $\Delta E'(d_{3/2}^{-1}f_{7/2})=7.37$ MeV. The difference in ΔE and $\Delta E'$ is accounted for by the average Coulomb-energy shift. The effective force parameter of the spin- and isospin-dependent Gaussian potential (central force) is 40 – 45 MeV and the oscillator parameter is 0.53. Isospin was not considered a good quantum number, thus their results showed strong T mixing. States with calculated level energies below 10 MeV are shown in Fig. 17 along

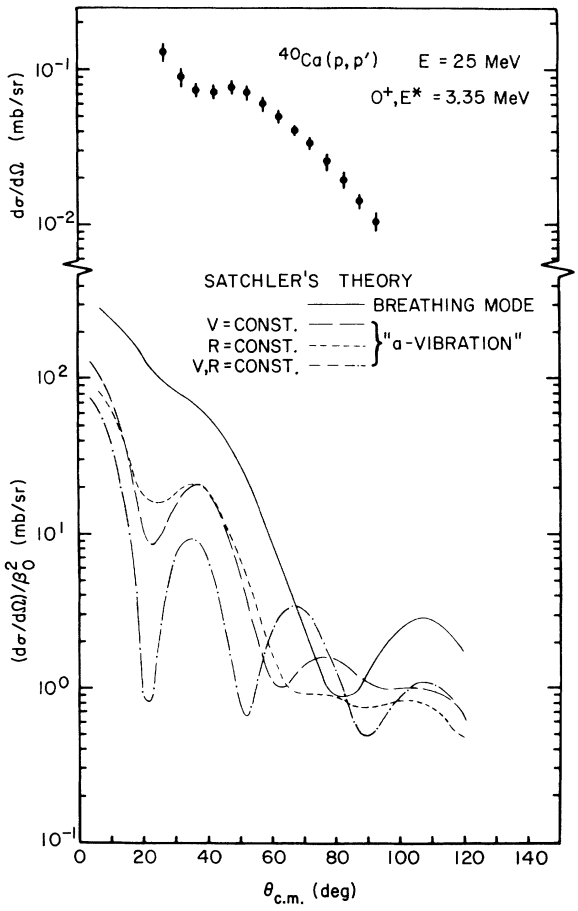

FIG. 17. Results of generalized collective-model calculations for the 0^+ excitation.

with the results of other investigations. However, Seth *et al.*[11] and Fuchs, Grabisch, and Roschert[12] found from proton stripping experiments that the odd-parity excited states of ^{40}Ca can be explained rather well by a simple shell model and that T mixing of low-lying states was much less than predicted. A summary of "configuration, spin, and isospin" assignments to the ^{40}Ca negative-parity states in terms of $(d_{3/2}^{-1}f_{7/2})$ and $(d_{3/2}^{-1}p_{3/2})$ shell-model states has been given by Fuchs, Grabisch, and Roschert.

In a pure RPA treatment of the odd-parity spectrum of ^{40}Ca, Kuo used a G matrix derived from the HJ potential for diagonalization. His spectrum is shown in the second column of Fig. 19 for the comparison with Gillet and Sanderson's results. Both RPA calculations encountered the difficulty of putting too much strength into the octupole transition to the ground state from the first 3^- state.

Dieperink's calculations used the modified surface δ interaction in both the RPA and Tamm-Dancoff approximation formulations, using a $(d_{3/2}^{-1}f_{7/2})$ splitting of 7.3 MeV. These diagonalized wave functions are very close to those of the unperturbed particle-hole states. The positions of the first four $T=1$ states were successfully predicted.

Gerace and Green[37] have constructed a model of mixing shell-model 1p-1h states mixed with 3p-3h deformed states to describe the odd-parity states of ^{40}Ca. Their procedure was to start with RPA wave functions which were obtained using $\Delta E(d_{3/2}^{-1}f_{7/2}) = 5.4$ MeV. Kuo's particle-hole matrix elements were used and the effects of core

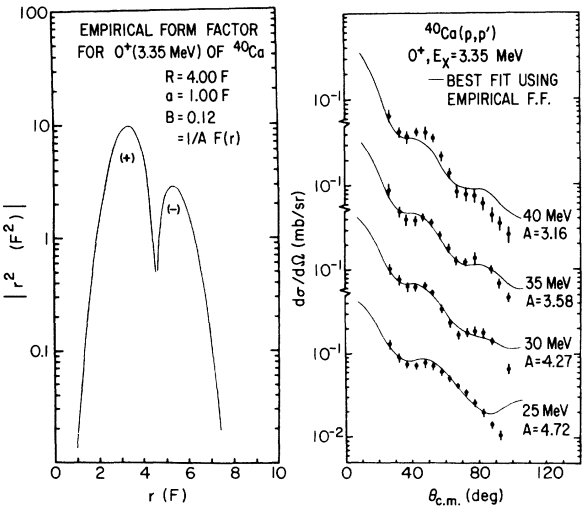

FIG. 18. The empirical form factor used in fitting the data. The solid curves are DWBA calculations using the empirical form factor and are shown in comparison with the data.

polarization were included. The 3p-3h deformed states were constructed by first coupling two Nilsson orbits to obtain a 1p-1h, $K=1$ wave function, then recoupling this to a 2p-2h wave function to get the 3p-3h wave function. Finally, matrix elements of the HJ potential between the $\langle 1\text{p-1h}|_J$ and $|\,3\text{p-3h}\rangle_J$ deformed states were obtained and the diagonalization was carried out. The diagonalized wave functions contain RPA wave functions and deformed $|\,3\text{p-3h}\rangle$ wave functions as illustrated in their paper. Their calculated spectrum is in good agreement with experimental levels below 8 MeV.

Fuchs, Grabisch, and Roschert have derived the spectroscopic factors for their (d,n) work using Gerace and Green's wave functions and assuming the ^{39}K ground state to be a pure $d_{3/2}$ hole. They found that this theory agreed with experiment very well except for a few discrepancies. Goode[46] has calculated several $E2$ decays for the low-lying $T=0$ odd-parity states of ^{40}Ca, and shown that a pure RPA description of these decays is not satisfactory, whereas Gerace and Green's picture provides a consistent explanation of the $B(E2)$ values. In comparison with the results of Goode's paper, several predictions of Gerace and Green were supported. For example, the deformed nature of the first 1^- state at 5.902 MeV and the predicted existence of the level sequence 3^-, 2^-, 4^- around 7 MeV are partially confirmed.

The purpose of this section is to summarize some of the current theoretical descriptions for the wave functions of the odd-parity states of ^{40}Ca, so that one can estimate the uncertainties in the DWBA calculations due to the wave functions used. In the present paper Kuo's wave functions were used. However, it now appears that Gerace and Green's wave function may be more accurate.

V. RESULTS AND DISCUSSIONS OF THE MICROSCOPIC DESCRIPTION

Calculations were performed for the first 1^-, $T=0$ state; first 2^-, $T=0$ and $T=1$ states; first, second, and third 3^-, $T=0$ states; first 3^-, $T=1$ states; first 4^-, $T=0$ and $T=1$ states; first 5^-, $T=0$ and $T=1$ states; and first 6^-, $T=0$ and $T=1$ states. The first 3^-, $T=0$; and first 5^-, $T=0$ states have also been investigated by Schaeffer and Petrovich.[39,40] Comparison with the results of these authors and discussion on the calculations in this paper will be presented in the following subsections.

1^-, $T=0$ State (6.948 MeV)

The major p-h components of the wave functions for the first RPA first 1^- state are $(2p_{3/2}d_{5/2}^{-1})$, $(2p_{3/2}d_{3/2}^{-1})$, and $(f_{5/2}d_{5/2}^{-1})$. The calculated an-

gular distributions at 40 and 25 MeV are best fitted by the distributions of the second experimental 1^- (6.948 MeV) state. Figure 20 shows good agreement both in shape and magnitude between theory and experiment if so assigned. Gerace and Green's calculations show that the first 1^- state is strongly deformed, whereas the second 1^- is a very pure 1^- shell-model state. Thus the assignment of the RPA first 1^- state to the second experimental 1^- state is supported by Gerace and Green's theory.

First 3 , T=0 State (3.736 MeV)

The ADW calculations for the lowest 3^- state (3.736 MeV) have been previously reported by Petrovich and McManus,[40] and Schaeffer.[39] The results of our calculations are shown in Fig. 21. For this 3^- state the magnitudes and positions of the maxima are well reproduced at each beam energy. The over-all shapes of the experimental distributions are also in qualitative agreement, which indicates that the energy dependence of the exchange effects has been correctly accounted for. It can be seen from Fig. 21 that the contributions from exchange become increasingly important at lower energies.

Calculations which use a 1-F range "KK equivalent" Yukawa force with an empirical strength

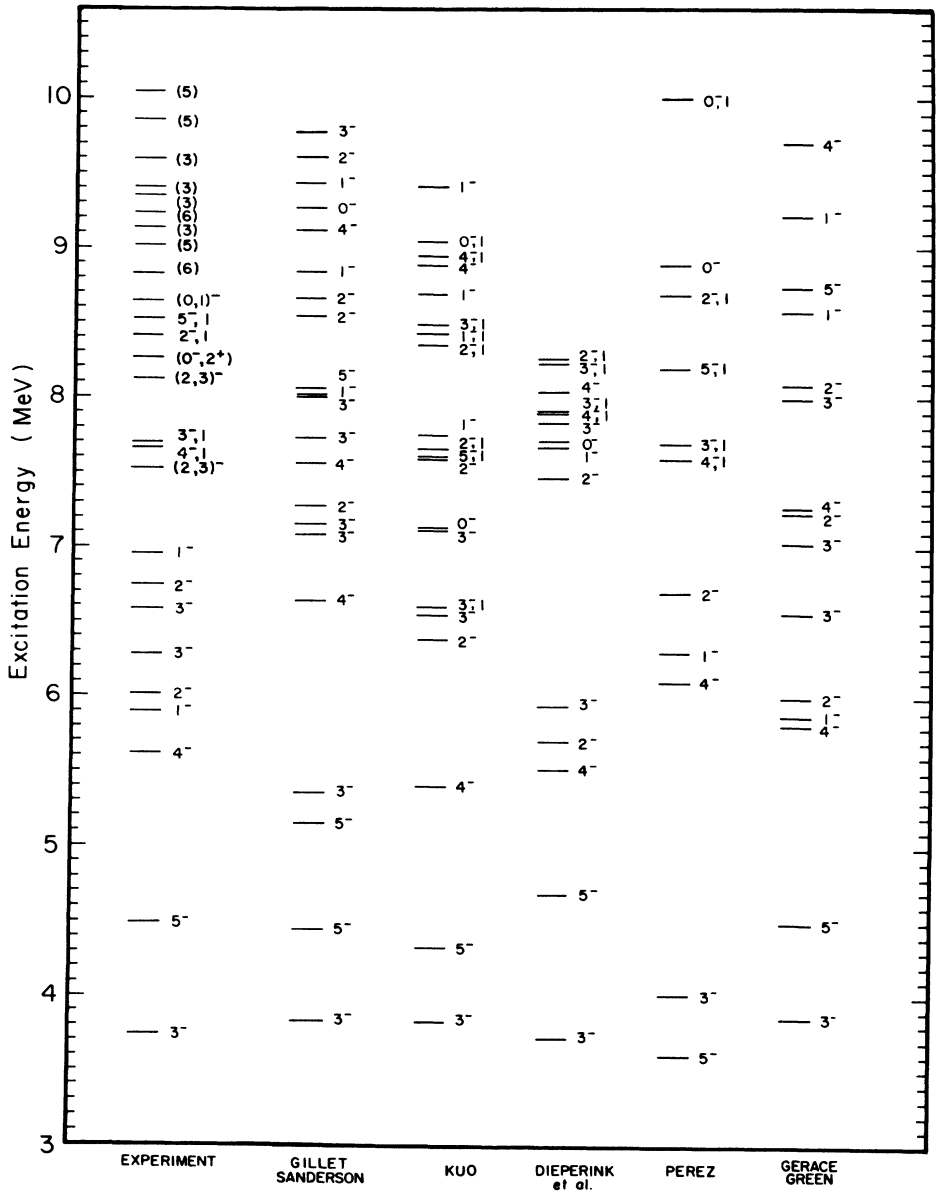

FIG. 19. Theoretical and experimental energy levels for negative-parity states of ^{40}Ca.

normalization are also illustrated in Fig. 21. The distributions are very similar to those obtained by using the KK+Ex force. The results of a central HJ force plus exchange are not shown because the shapes of the calculated distributions (indirect, exchange, and total) were found identical to those using KK+Ex forces, except that the predicted magnitudes were found to be about 25% lower. This similarity also applies to the calculations for the second 3^- (6.285 MeV) and the 5^- (4.491 MeV) states.

Schaeffer[39] has performed similar calculations for ^{40}Ca with proton energies from 17.3 to 55 MeV. He used the Blatt-Jackson potential and Gillet and Sanderson's wave functions. The dependence of exchange effects upon the energy was investigated by examining the ratio of the total cross section $\sigma(D+E)$ to the direct cross section $\sigma(D)$. A comparison of the results of his calculations with those obtained in this work are given in Table IX.

Second and Third 3^-, $T=0$ States (6.285 and 6.581 MeV)

Figure 22 shows the results of the calculations for the 6.285-MeV state using direct, exchange, and a direct-plus-exchange force. The experimental cross sections are again well reproduced except at 40 MeV and at large angles where the exchange contributions are overestimated.

A comparison of the experimental angular distributions between this 3^- and the first 3^- state reveals some differences which may be attributed to the nuclear wave functions or to the mechanism of the interaction or both. The agreement between the ADW calculations and the experimental results seems to suggest that the RPA descriptions for this state are quite good. However, difficulties were encountered when the ADW calculations for the third RPA 3^- state were compared with the distributions of the third 3^- of the experimental spectrum. It was found that the calculated cross sections were 10 times too low, as can be seen in the comparison between Fig. 12 and Fig. 23. On the other hand, this discrepancy was resolved in the extended shell-model calculations of Gerace and Green,[4] their third 3^- state is essentially the second RPA 3^- state and their second 3^- state is a mixture of the 3p-3h deformed state as well as contributions from the first and the second RPA 3^- states. The electric transition rates to the ground state from second and third 3^- states of Gerace and Green are about equal (1.9 vs 2.7 s.p.u.), thus their picture is consistent with the excitation strength measured in this experiment (2.5 vs 1.7 s.p.u.).

5^-, $T=0$, 1 States (4.491 and 8.535 MeV)

The ADW calculations using Kuo's wave func-

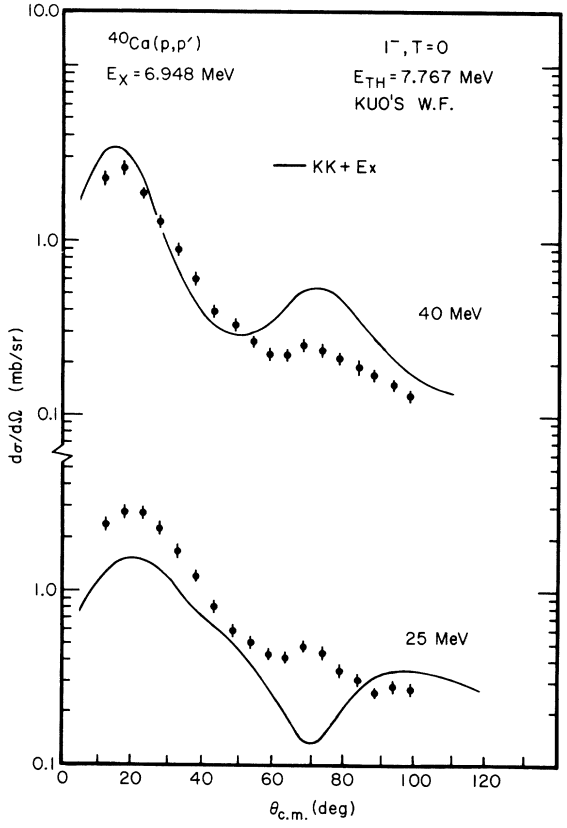

FIG. 20. Microscopic DWBA calculations for the 1^-, $T=0$ state.

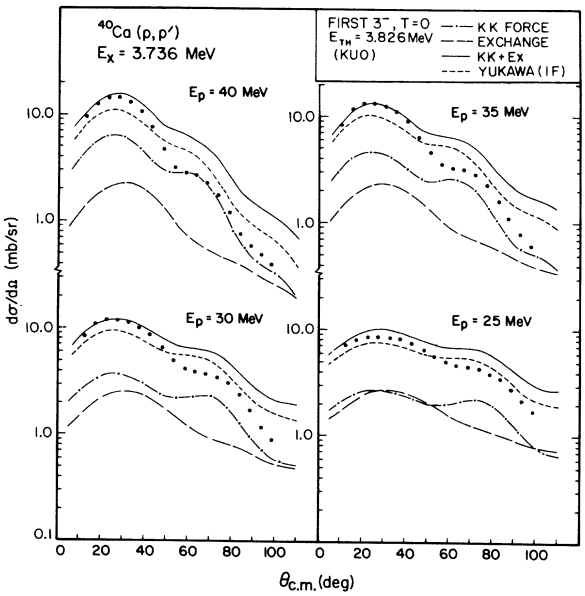

FIG. 21. Microscopic DWBA calculations for the first 3^-, $T=0$ state.

tions for the 5^-, $T=0$ (4.491 MeV) state are shown in Fig. 24. The exchange term dominates the contribution to give the correct magnitude of the differential cross sections but overshoots somewhat at large angles. The contributions from the direct term are small as can be seen from Fig. 24 and the $\sigma(D+E)/\sigma(D)$ ratio in Table IX. The ADW calculations for this state demonstrate the extreme importance of the exchange effect in predicting the correct magnitude of the angular distributions.

The calculated distribution of the first 5^-, $T=1$ state using Kuo's wave functions is shown in Fig. 23. The distributions of the components $LSJ=505$ and 515 were found comparable in magnitude. The total distribution is the incoherent sum of these two components. The corresponding experimental results show that the calculations predict the correct normalization.

The particle-hole configurations of these RPA 5^-, $T=0$ and 1 states are mainly $(f_{7/2}d_{3/2}^{-1})$, in good agreement with the results of (^{3}He, d) and (d,n) measurements (Refs. 12–14) and with the theory of Gerace and Green.[4]

Unnatural-Parity States

The ADW calculations were done using Kuo's wave functions for the 2^-, $T=0$ state (6.026 MeV) at four energies, and for the 2^-, $T=1$ state (8.418 MeV) at 25 and 40 MeV. The results are illustrated in Fig. 25. At $E_p=40$ MeV, both $T=0$ and $T=1$ states are qualitatively reproduced . At the lower energies the calculations systematically underestimate the differential cross sections at small angles. Because of the similarity both in shape and cross section, this experiment could not distinguish between the RPA and deformed 2^-, $T=0$ states. This leaves an ambiguity in this experiment in the interpretation of the states at 6.026 and 6.751 MeV.

The results for the first 4^-, $T=0$ and $T=1$ states are shown in Fig. 23. The predicted differential cross section for the 4^-, $T=0$ state is about 20 times lower than the experimental results of the 5.617-MeV state (see Fig. 14). On the other hand, this theoretical distribution resembles in shape the experimental counterpart. For the 4^-, $T=1$ state, the predicted magnitude of the cross section is about $\frac{1}{2}$ of the estimated experimental results (the 4^-, $T=1$ level at 7.656 MeV was not resolved, but a few clean spectra enabled the estimation of the cross section to be made). It is also noted that both calculated distributions of the 4^-, $T=0$ and $T=1$ are similar.

Results for the 6^-, $T=0$ and $T=1$ states were also obtained as shown in Fig. 23. The experimentally observed level at 8.850 MeV ($L_p=7$) may be assigned to the theoretical 6^-, $T=1$ state. The assignment of the 9.237-MeV $L=7$ level to the theoretical 6^-, $T=0$ state is also plausible, because the predicted differential cross sections are for this state close to those of the 9.237-MeV level. Both of these states are predicted to have excitation energies between 12 and 13 MeV in the microscopic calculations. However, the experi-

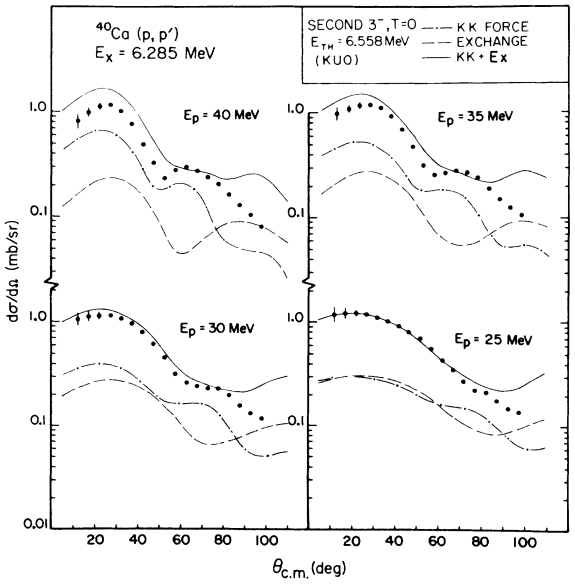

FIG. 22. Microscopic DWBA calculations for the second 3^-, $T=0$ state.

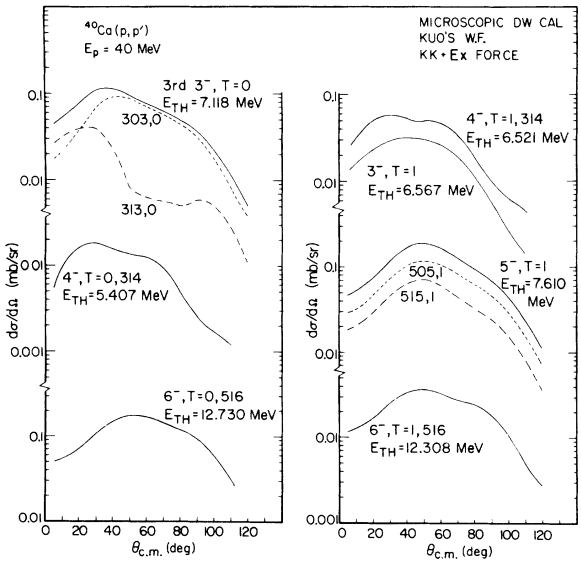

FIG. 23. Microscopic DWBA calculations for the third 3^-, $T=0$; first 3^-, $T=1$; first 4^-, $T=0$, 1; first 4^-, $T=1$; and 6^-, $T=0$, 1 states.

mental excitation energies are approximately consistent with their being the 6^- states of a rotational band starting at the 5.902-MeV 1^- state.

The RPA wave functions of the unnatural-parity states used above can all be qualitatively described as pure single particle-hole states. They are

RPA first 2^-, $T=0$ $f_{7/2}d_{3/2}^{-1}$,

RPA first 2^-, $T=1$ $2p_{3/2}2s_{1/2}^{-1}$,

RPA first 4^-, $T=0,1$ $f_{7/2}d_{3/2}^{-1}$,

RPA 6^-, $T=0,1$ $f_{7/2}d_{5/2}^{-1}$.

The similarities in the wave functions of the 4^- and 6^- states, as well as the differences between the 2^-, $T=1$ states are also reflected by the calculated distributions, as expected. Gerace and Green's deformed model agrees with the RPA description of the first 4^- state. This ($f_{7/2}d_{3/2}^{-1}$) configuration has been confirmed by Erskine,[45] Seth *et al.*,[11] and Fuchs, Grabisch, and Roschert[12] in their (^{3}He, d) and (d,n) experiments, respectively. Thus the wave functions of this state are believed to be well understood. The failure of ADW calculation for this particular state must be due to the effective force used. Perhaps the tensor force or spin-orbit force will play an important role in regaining the correct normalization. For example, it was found by Love[43] in calculating ^{90}Zr(p,p') cross sections that the highest spin transfer was dominated by the two-body spin-orbit interaction. The spin-orbit force is also important[47] in the excitation of the unnatural-parity z state at 8.87 MeV in ^{16}O.

Even-Parity States

Figure 26 shows all of the even-parity states observed in this experiment. The spacing between the vertical lines is in accord with a $J(J+1)$ relationship. The length of the horizontal lines is proportional to the transition strength. The open circles are for those states observed in other experiments (see Table X).

The low-lying even-parity states of ^{40}Ca have been described in terms of multiparticle-multihole configurations by Gerace and Green[37,48] and by Federman and Pittel.[49,50]

In the paper[37] of Gerace and Green some of the low-lying states are considered as mixtures of the double closed $2s$-$1d$ shell-model state ($j=0$) with two intrinsic deformed states (containing components with even angular momenta) formed by raising two and four particles from the $1d_{3/2}$ shell into the $2p$-$1f$ shell. Their results are shown in Table XI. The first calculated sequence appears to correspond to the experimentally observed 3.350 (0^+), 3903 (2^+), and 5.279 (4^+) states, which seem to form a nearly perfect rotational band (see Fig. 26). In the second calculated sequence, the 8.00-MeV level may be either the observed 7.923- or 8.100-MeV level. This 2p-2h sequence does not follow the $J(J+1)$ relationship and no discussion of this aspect was given. Gerace and Green[48] also used their deformed model and mixing technique to account for the 5.212- (0^+) and 5.249-MeV (2^+) states. K-band mixing and 6p-6h, 8p-8h deformed rotational bands were included. Their previous calculations were modified

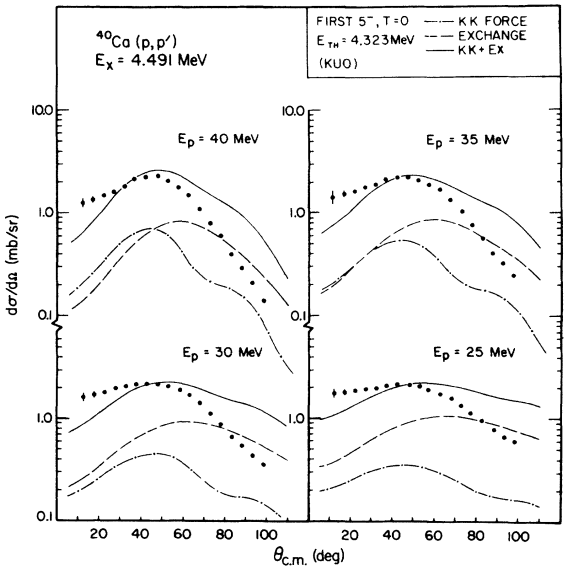

FIG. 24. Microscopic DWBA calculations for the first 5^-, $T=0$ state.

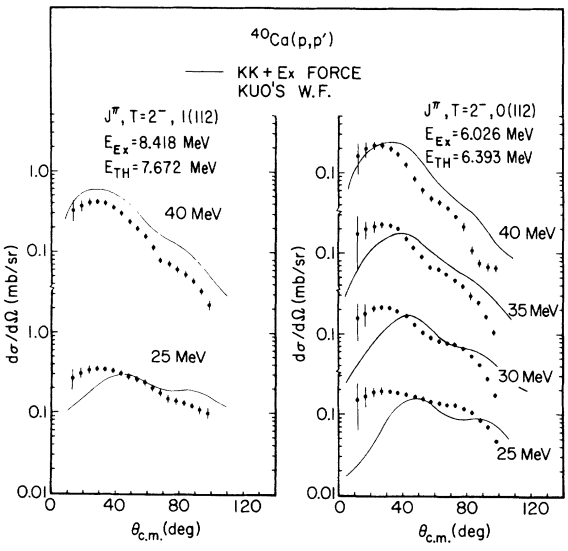

FIG. 25. Microscopic DWBA calculations for the first 2^-, $T=0$ state.

to allow complete mixing between 0p-0h, 2p-2h, 4p-4h, 6p-6h, and 8p-8h configurations. Anderson *et al.*[51] compared their $(p,p'\gamma)$ results with Gerace and Green's picture. A $K=2$, 4p-4h band for 5.249- (2^+), 6.026- (3^+), and 6.505-MeV (4^+) levels, and a $K=0$ 8p-8h band for 5.249- (0^+), 5.627- (2^+), and 6.544-MeV (4^+) levels were constructed based on the enhancement of the in-band transitions. The former band does not obey the $J(J+1)$ law, whereas the latter does (see Fig. 26). Anderson *et al.* found that there was a general agreement between the experimental reduced matrix elements and the theoretical values for the 4p-4h and 8p-8h states.

Federman and Pittel[49] have shown that an alternative description for the low-lying 0^+ levels of ^{40}Ca is possible which does not require a 6p-6h or 8p-8h state. They proposed a weak-coupling model in which the energies of the known 0^+ states are 3.29, 5.22, and 7.62 MeV, in excellent agreement with the experimental 0^+ states at 3.350, 5.212, and 7.300 MeV. The same model was also applied to the 2^+ states[52] and all eight 2^+ states were well reproduced by the calculated spectrum. It should be noted that Gerace and Green's model attempted to retain the band structure of the deformed even-parity states, whereas Federman and Pittel's model emphasized only the configurations of the spectrum of a given even J; thus no calculation was made for 4^+ states. These two models have enjoyed success in different areas and a comparison between them can only be made by an experiment of electromagnetic transitions between those states covered by both areas of studies.

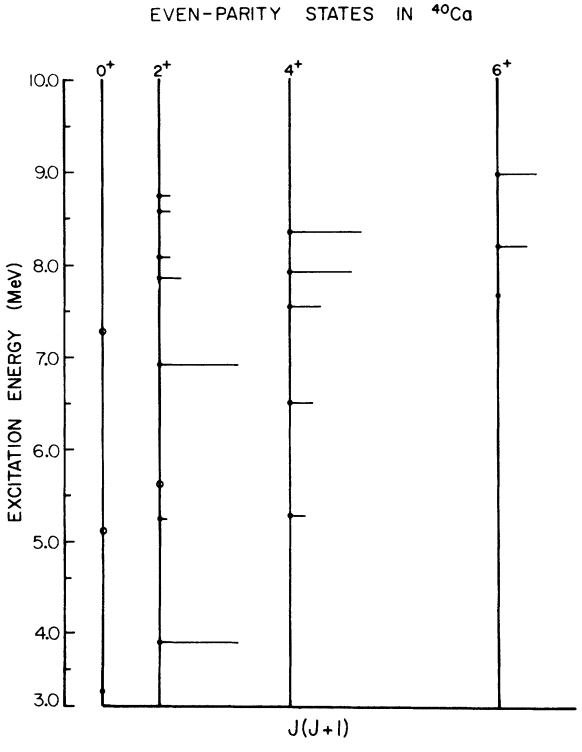

FIG. 26. Systematics of the even-parity states in ^{40}Ca observed in this experiment. Open circles are those from other experiments.

So far, all the observed 0^+ and 2^+ states and those 4^+ states below 7 MeV have been theoretically investigated. However, the 4^+ states above 7 MeV and the 6^+ states in this experiment may bring new information out of the band structures of the even-parity states in ^{40}Ca. Further theoretical and experimental studies on this aspect are desired.

First Excited 0^+ State (3.350 MeV)

There is a general agreement between the Gerace and Green and the Federman and Pittel models that the 3.35-MeV level in ^{40}Ca is mainly a 4p-4h deformed state. The 4p-4h strength predicted is about 70% by Gerace and Green model and is about 83% by Federman and Pittel model. The ^{42}Ca(p,t)-^{40}Ca experiment[52] showed that if the ground state of ^{40}Ca is assumed to be a pure 0p-0h (shell-model) state, the 3.350-MeV 0^+ state is certainly not a pure 2p-2h state. This evidence complements the Gerace and Green and Federman and Pittel results.

The configuration of the ground state of ^{40}Ca is described mainly by 0p-0h (82%) mixed with 2p-2h (17%). This mixture has been supported by ^{40}Ca(p,d), ^{40}Ca$(^3$He$,^4$He) reactions[53] and also by the ^{39}K$(^3$He$,d)$ experiment.[11] If one compares the wave functions of the ground state and those of the first excited 0^+ state predicted by the Gerace and Green model, such as

Ground state: 0p-0h(0.91), 2p-2h(0.41);

3.35-MeV state: 4p-4h(−0.83), 6p-6h(−0.45),

one finds that the 3.35-MeV state might be predominantely a 4p-4h excitation from the ground state as a whole.

In Sec. III, it was mentioned that the (p,p') data obtained in this experiment could only be fitted using an empirical form factor shown in Fig. 18, and that the fit is very sensitive to the relative size of the oscillation in the surface. If a form factor, calculated by using 4p-4h wave functions and appropriate effective interaction, could be obtained, it would be interesting to see the comparison between this theoretical form factor with the empirical one.

An alternate possibility for explaining the observations on the 0^+ state may lie in a two-step process such as picking up two neutrons in the

spherical ground state and returning them to the deformed excited 0^+ state. At 40 MeV the reaction $^{40}Ca(p, t)^{38}Ca(g.s.\ 0^+)$ has a similar angular distribution.[54] The main difference is that the (p, t) angular distribution has a deeper valley than does the inelastic scattering presented here.

VI. COMPARISONS WITH OTHER EXPERIMENTS

Energy Levels

Figure 27 presents the levels seen in this (p, p') experiment along with representative spectra from other types of reactions. The energies of the low-lying levels have been determined with high precision by high-resolution (p, p')[54,27] and γ-ray measurements.[55,28,29] The energies given in this work were obtained by a calibration which used Grace and Poletti's results.

As can be seen from Fig. 27, there is good agreement between the results of the present experiment and that of Grace and Poletti from 3.350- to 8.850-MeV excitation energy. The 5.212- and 6.544-MeV states were too weakly excited to be

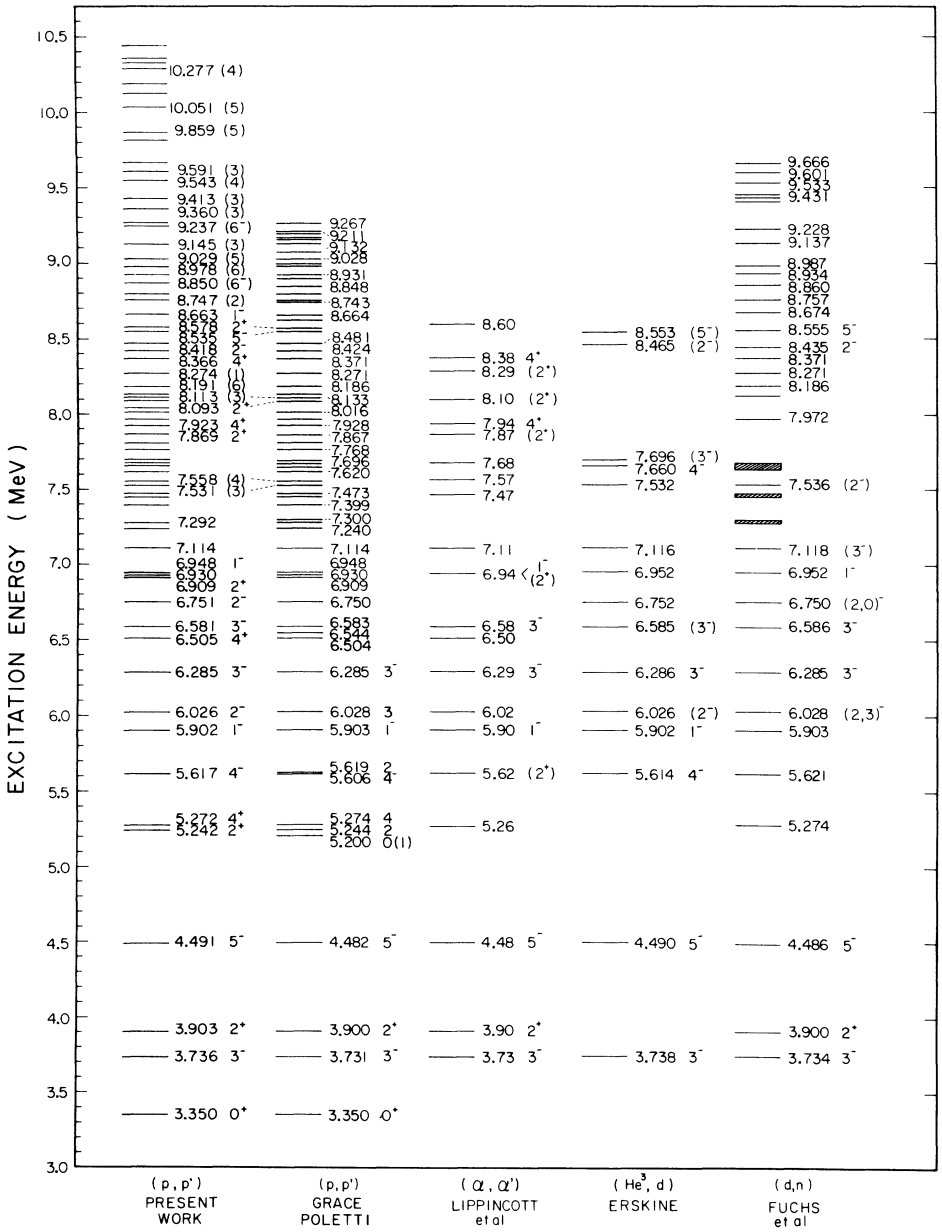

FIG. 27. Energy levels of ^{40}Ca observed by various experiments.

TABLE X. Spin and parity assignments of states in ^{40}Ca.

Refs.: a	b		(p,p') 25-40 MeV b	(p,p') 55 MeV c	(p,p') 17 MeV d	(α,α') 51 MeV e	(α,α') 31 MeV f	(e,e') 120-220 MeV g	(e,e') 20-60 MeV h	$(^3\mathrm{He},d)$ 12 MeV i	$(^3\mathrm{He},d)$ 14 MeV j	(d,n) 6 MeV k	(p,γ) l	(p,γ) m	$(p,p'\gamma)$ 7.9-9.6 MeV n	$(p,p'\gamma)$ 9 MeV o	$(p,p'\gamma)$ 8-10 MeV p	$(p,p'\gamma)$ 12 MeV q	γ Res r	Probable assign.
E^*(keV)	$E^*\pm\Delta E$(keV)		L	L	L	J^π	J^π	J^π	J^π	J^π	J^π	J^π	J^π	J^π	J^π	J^π	J^π	J^π	J^π	J^π
3350	3350														0^+	0^+	0^+			0^+
3737	3736	1	3	3	3	3^-	3^-	3^-	3^-	3^-	3^-	3^-	3^-	3^-	3^-	3^-	3^-			3^-
3904	3903	1	2		2	2^+	2^+	2^+	2^+				2^+	2^+	2^+	2^+	2^+			2^+
4492	4491	1	5	5		5^-	5^-	5^-		5^-	5^-	5^-	5^-	5^-	5^-	5^-	5^-			5^-
5212															0, (1)	0^+	0^+			0^+
5249	5263	6	2			( )$^-$							2	2	2	2^+	2^+			2^+
5279			4										4^+	4^+	4	4^+	4^+			4^+
5615	5617	3	5			( )$^-$	(2^+)			4^-	4^-	4^-	4^-	4^-	$4^{(-)}$	4^-	4^-			4^-
5627														2	2	2^+	2^+			2^+
5900	5902	4	1			3^-	1^-			1^-	1^-	1^-			1^-	1^-	1^-			1^-
6025	6026	3	3							(2^-)	(2^-)	$(2,3)^-$			3, (2)	2^-	2^-			2^-
6029																3^+	3^+	(3^+)		(3^+)
6285	6285	1	3		3	3^-	3^-	3^-		3^-	3^-	3^-	3^-		3^-	3^-	3^-			3^-
6509	6505	6	4		3												4^+			4^+
6544																	4^+			4^+
6585	6581	2	3			3^-	3^-			(3^-)	3^-	3^-					3^-			3^-
6750	6751	4	3							( )$^-$	$(2,0)^-$	$(2)^-$			(3)$^-$					$(2)^-$
6909	6909	5	2	2+3	2	$2^+ + 3^-$	(2^+)	$(2^+ + 3^-)$	$(2^+ + 3^-)$				(1, 2)					(2^+)	2^+	2^+
6930			(≥3)			$2^+ + 1^-$												(3^-)		(3^-)
6948	6948	5	1				1^-			( )$^-$	1^-	1^-						(1^-)	1^-	1^-
7114	7114	1	5		3					( )$^-$	$(3)^-$	3^-						$(2^+), (3^-)$		?
7280	7292	5	(0, 2)																	
7300													0					0^+		(0^+)
7455	7455	5	4																	(4^+)
7473														2				(2^+)		(2^+)
7531	7543	5	3								$(2)^-$	$(2)^-$								$(2)^-$
7558			(4)											<5						(4^+)
7655										4^-	4^-									4^-
7676	7673	8	(≥6)																	(≥6)
7696										$(3)^-$	3^-									3^-
7867	7869	4	2				(2^+)											(2^+)		2^+
7928	7923	6	4			4^+	4^+													4^+
8092	8100	5	2			2^+	2^+											(2^+)		2^+
8113			3															(1^-)		$(1,2,3)^-$
8186	8191	5	(6)																	(6^+)

TABLE X *(Continued)*

Refs.: a	b		(p, p′) 25-40 MeV b	55 MeV c	17 MeV d	(α, α′) 51 MeV e	31 MeV f	(e, e′) 120–220 MeV g	20–60 MeV h	(^{3}He, d) 12 MeV i	14 MeV j	(d, n) 6 MeV k	(p, γ) l	m	(p, p′γ) 7.9-9.6 MeV n	9 MeV o	8-10 MeV p	12 MeV q	γ Res r	Probable assign.
E^*(keV)	$E^* \pm \Delta E$(keV)		L	L	L	J^π	J^π	J^π	J^π	J^π	J^π	J^π	J^π	J^π	J^π	J^π	J^π	J^π	J^π	J^π
8271	8274	6	1				(2^+)											$(0^-), (2^+)$		$(0^-, 2^+)$
8371	8366	6	4			4^+	4^+													4^-
8424	8418	4	3							(2^-)	2^-	2^-								2^-
8535	8564	6	5			2^+		5^-		(5^-)	5^-	5^-								5^-
8578			2															(2^+)		2^+
8743	8747	6	2															(1^-)		$(1^-, 2^+)$
8848	8850	4	7																	(6^-)
8977	8978	6	6																	(6^+)
8993																		(2^+)		2^+
9028	9029	5	5																	
9132	9145	5	3																	
9158																				
	9237	3	7																	(6^-)
	9360	5	3																	
	9413	5	3									$(3)^-, (2)^-$	2							$(3)^-, (2)^-$
	9541	5	4										1^-							
	9591	4	3																	
	9642	6											2^-							2^-
	9859	4	5										1							
	10051	3	5									$(0)^-$								
	10277	3	4																	

[a] Reference 13.
[b] Present experiment.
[c] Reference 65.
[d] Reference 60.
[e] Reference 8.
[f] Reference 7.
[g] Reference 9.
[h] Reference 10.
[i] Reference 45.
[j] Reference 11.
[k] Reference 12.
[l] Reference 57.
[m] References 29, 58.
[n] Reference 27.
[o] Reference 28.
[p] Reference 56.
[q] Reference 13.
[r] Reference 59.

TABLE XI. Deformed-state calculations of Gerace and Green.

Main configuration	0^+	2^+	4^+
4p-4h (mixed with 2p-2h)	3.55 MeV	3.90	5.25
2p-2h (mixed with 4p-4h)	7.33 MeV	6.90	8.00

seen in this experiment. Above 7 MeV, the (α, α') experiment recorded only a few levels due to experimental limitations.

Spin Identification

The J^π assignments of the excited states of ^{40}Ca obtained from various experimental sources are summarized in Table X. Some of this information has been reported by Seth *et al.*[11] Since then many new results on spin assignments for the excited levels of ^{40}Ca, including those from this experiment, have become available.

States Below 6.58 MeV

The spins and parities of low-lying levels below 6.58 MeV have been well determined. The most complete set of spin assignments was given by Anderson *et al.*[51] who have done extremely precise $(p, p'\gamma)$ measurements. A summary of the previous assignments has been discussed by Seth *et al.*[11] The spins and parities of 3.350- (0^+), 3.736- (3^-), 3.903- (2^+), 4.491- (5^-), 5.617- (4^-), 5.902- (1^-), 6.026- (2^-), 6.285- (3^-), and 6.581-MeV (3^-) excited states are consensus assignments. Of the triplet at 5.212-5.249-5.279-MeV the 5.212 state, which was not seen in this experiment, has been identified as 0^+ by all of the most recent $(p, p'\gamma)$ studies.[28, 52, 56]

Individual angular distributions for the 5.249- and 5.279-MeV states were obtained (see Figs. 11 and 13) and are assigned $L=2$ and $L=4$. The assignments are in agreement with results of (p, γ) and $(p, p'\gamma)$ experiments.[57, 5, 58]

The 5.627-MeV component of the 5.617-MeV doublet has been identified as 2^+ by many γ-decay experiments. In this work, the angular distributions of this doublet permit a small mixture of $L=2$ strength to the dominant $L=5$ strength. The upper limit of the $L=2$ contributions was determined to be ($\delta_2 \lesssim 0.09$). The value of $B(E2)$ in Weisskopf units, i.e., $G(\mathrm{sp})$, based on this estimated deformation is in qualitative agreement with other electromagnetic transition measurements. On the other hand, the (α, α') experiment by Lippincott and Bernstein[7] observed only the 2^+ component, indicating that this state is observed in both types of inelastic scattering.

The 6.029-MeV level of the 6.025-6.029-MeV doublet was discovered by Grace and Poletti. It is assigned as having $J=3^+$, but 2^- was not entirely ruled out according to Anderson *et al.* In the present experiment, this doublet was observed to be an $L=3$ transfer as a whole.

Anderson *et al.* are the only group who identify the 6.544-MeV level as 4^+. In the present experiment the 6.505-MeV level was well resolved from the 6.581-MeV state (see Fig. 2) and found to be a 4^+ state. However, the 6.544-MeV level was not seen at all. It may be the case that this state was weakly excited with respect to the 6.505-MeV level and because it is also a 4^+, the analyzed group may actually be a 4^+-4^+ doublet.

States Between 6.750- and 7.558-MeV Excitation Energy

6.751-MeV level. This state has been assigned as $(2, 0)^-$. Seth *et al.*,[11] working in the ^{39}K(^{3}He, d) reaction prefer 0^-. However, Fuchs, Grabisch, and Roschert, who have done the ^{39}K(d, n) experiment[12] to unfold the problem of the missing 2^- strength of the $T=0$ quartets of the $(d_{3/2}^{-1} f_{7/2})$ and $(d_{3/2}^{-1} p_{3/2})$ configurations, contend that this 6.751-MeV state should be assigned as 2^- based on an observed $L=3$ transition, as opposite to the $L_p=1$ assignment obtained by Seth *et al.* They interpret this state as the 2^- component of the $(d_{3/2}^{-1} f_{7/2})$ quartet. In the present (p, p') experiment, the 6.751-MeV level was observed to be excited by an $L=3$ transfer indicating that the (p, p') reaction favors the 2^- assignment or possibly 3^- (see Fig. 12). Resolution of the discrepancy between the contradictory results of the (d, n) and $(^3\mathrm{He}, d)$ reactions can be found partly from Gerace and Green's calculations[4] based on the mixing of 3p-3h deformed states with the shell-model states of Kuo.[3]

The wave function of the second 2^- state from Gerace and Green's calculations shows that it contains about 29% of $|3\mathrm{p}\text{-}3\mathrm{h}\rangle$, and 69% of $\psi_1^{2^-}$ (Kuo), in which $(d_{3/2}^{-1} f_{7/2})$ is the largest component.[3] Hence the theoretical configurations proposed for the second 2^- state are (deformed) plus the $(d_{3/2}^{-1} f_{7/2})$. The predicted energies for the first and second 2^- states are 6.4 and 6.185 MeV which closely agree with the experiment values of 6.026 and 6.751 MeV if the latter is assigned to 2^-. The agreement between theory, (d, n), and this (p, p') experiment suggests that the 2^- assignment is favored for the 6.751-MeV state.

6.909-6.930-6.948-MeV triplet. Individual angular distributions for the 6.909- and 6.948-MeV states were obtained and their L transfers are positively assigned as 2 and 1 (see Figs. 11 and

TABLE XII. Comparison of nuclear deformations, δ_L (F).

E[a] (MeV)	L	(p,p') This experiment 40 MeV	(p,p') This experiment 25 MeV	(p,p') Ref. 60 17 MeV	(p,p') Ref. 65 55 MeV	(α,α') Ref. 8 50 MeV	(α,α') Ref. 7 31 MeV	(e,e') Ref. 9 120–220 MeV
3.736	3	1.32	1.40	1.44	1.32	0.85	1.35	0.84
3.903	2	0.43	0.42	0.40		0.34	0.55	0.48
4.491	5	0.80	0.91		0.68	0.35	0.71	0.40
6.285	3	0.40	0.46	0.52		0.40	0.71	0.23
6.581	3	0.32	0.41	0.60		0.31	0.54	
7.114	5	0.27	0.40	0.68[a]				
7.869	2	0.23	0.28				0.44	
7.923	4	0.29	0.34			0.29	0.53	0.40
8.366	4	0.32	0.32			0.24	0.47	
8.535	5	0.18	0.23					0.31
8.578	2	0.14	0.17			0.19		

[a] $L=3$ was used.

16). Metzger,[59] using γ-resonance absorption techniques has concentrated his effort on this triplet, and he identified the first and third members as 2^+ and 1^-. The 6.948-MeV level has also been assigned 1^- by proton stripping reactions. As has been mentioned in Sec. II, where the analysis of this triplet was discussed in detail, the middle level of 6.930 MeV may be a high-spin state (≥ 3).

7.114 level. The spin and parity of this state has been tentatively assigned $(3)^-$ by many authors. This assignment was first given by Gray, Kenefick, and Kraushaar[60] in a (p,p') experiment. This level was also observed by the (α,α') reaction[7] although no spin identification was made. An $L=1$ transition observed for this state in $(^3\mathrm{He},d)$[46,11,61] and (d,n)[12] reactions leads to the $(3)^-$ assignments by these authors.

A contradictory result was found in the present (p,p') experiment. The angular distributions of this state resemble those having $L=5$ transfer and are very similar to those of the 5.617-MeV state (see Fig. 14). At $E_p=25$ MeV, the distributions of these two levels agree very well with the $L=5$ collective model prediction. At $E_p=40$ MeV, the distribution is intermediate between $L=5$ and $L=4$. In any case, the angular distributions of the 5.617- and 7.114-MeV states are remote from those of $L=3$ transfer. Other evidences of similarity between these two levels can be seen from the $^{39}\mathrm{K}(p,\gamma)$ experiment performed by Lindeman *et al.*[58] The γ-ray branchings of both the 5.617- and 7.114-MeV levels were found to be about the same, namely 70% to the 3.74-MeV level and 30% to the 4.49 level.

The forementioned calculations by Gerace and Green suggest that the second 4^- state is essentially a collective state with over 80% of 3p-1h strength. The predicted energy is 7.65 MeV. Thus it is possible that the 7.114-MeV level corresponds to the second 4^- of Gerace and Green's scheme. The $L=1$ stripping transition to this state cannot, perhaps, be interpreted by the simple particle-hole picture of the shell model. The present data on the 7.114-MeV state are most consistent with a 4^- assignment but the disagreement with the proton stripping remains unresolved.

7.543-MeV doublet. The 7.531-MeV state has been observed in $(^3\mathrm{He},d)$ and (d,n) experiments and tentatively assigned as $(2)^-$, based on the shell model. In the present experiment, this and the 7.558-MeV levels are not separated and were analyzed by decomposition (Sec. II). The 7.531-MeV

TABLE XIII. Comparisons of reduced transition probabilities, G(sp) in Weisskopf single-particle units.

Transition (100% or 100%)	(p,p') Present 40 MeV	(e,e') Ref. 10	(e,e') Ref. 9		$(p,p'\gamma)$ Ref. 28	$(p,p'\gamma)$ Ref. 52	$(p,p'\gamma)$ Ref. 56
3^-(3.736) 0^+(g.s.)	28.7 ±2.0	31.7	7.4±0.8		20.7 ±5.1		
2^+(3.903) 0^+(g.s.)	2.05±0.2	2.0	2.4±0.75	4±1.3[a]	2.47±0.82	1.6±0.5	1.7
2^+(5.429) 0^+(g.s.)	0.26±0.05				0.12±0.02		1.1
2^+(6.909) 0^+(g.s.)	2.25±0.23	1.7	2.7±0.3	1.7[b]		1.7±0.15	4

[a] Reference 56.

[b] Reference 61.

level is found to be excited by an $L=3$ transfer in agreement with the results of proton stripping reactions. The 7.558-MeV state is identified as an $L=4$ transfer. The 7.57-MeV level observed in the (α, α') experiment[7] may correspond to this state.

$T=1$ Analog States

The $T=1$ analog states of ^{40}K have been assigned by Erskine at 7.655 (4^-), 7.696 (3^-), 8.414 (2^-), and 8.535 MeV (5^-). His proposal was based on the results of his (^{3}He, d) data and on Enge's (d, p) experiments[45,62] and of the observation of the lowest $T=1$ state in ^{40}Ca by Rickey, Kashy, and Knudsen.[63] The energy of this state has also been measured by Kashy and Snelgrove.[64] These experimental results also agree with the calculated excitation for the lowest ^{40}K analog states in ^{40}Ca in the $(d_{3/2}^{-1}f_{7/2})$ configuration. Experimentally, this has been further investigated by Seth *et al.* and Fuchs, Grabisch, and Roschert. Both groups have confirmed Erskine's identification. Fuchs, Grabisch, and Roschert even extended this technique to identify the $T=1$, $(d_{3/2}^{-1}p_{3/2})$ quartet.

In the present experiment, the 7.655-7.676-7.696-MeV triplet was not resolved and the J^π values of the 7.655- and 7.696-MeV states are taken from the results of authors mentioned above. The 8.418- and 8.535-MeV levels are observed to be $L=3$ and 5 transitions, respectively, consistent with the 2^- and 5^- results of the stripping reaction experiments. The $(d_{3/2}^{-1}p_{3/2})$ $T=1$ quartet was proposed by Fuchs, Grabisch, and Roschert to consist of the 10.051- (0^-), 9.435- (1^-), 9.408- (2^-), and 9.404-MeV (3^-) levels. At $E_p=35$ MeV, a level at 10.051 MeV is seen having $L=5$ transfer. No angular distribution for the 9.435-MeV state was obtained here. A doublet at 9.413 MeV with an $L=3$ angular distribution was observed which could possibly correspond to the 2^- and 3^- levels at 9.408 and 9.404 MeV. The other (p, p') experiments[60,65] have not observed these states.

States Between 7.6 and 8.8 MeV

Aside from the $T=1$ analog states discussed in the last section, there are a few even-parity states which lie in this region. The 7.869-, 8.092-, 8.578-, and 8.747-MeV levels were identified as having an $L=2$ transfer and the 7.923- and 8.366-MeV levels as $L=4$, in agreement with the results of (α, α') experiments. It is interesting to observe from Table X that the (α, α') experiments excited none of the $T=1$ states as expected from the selection rule $\Delta T=0$ for the inelastic scattering of α particles.

There are two $L=1$ states observed in this region. The 8.274-MeV level (see Fig. 16) is tentatively assigned as a doublet with possible spins of (0^-) and (2^+). The 0^- component of the $T=0$ $(d_{3/2}^{-1}p_{3/2})$ quartet was tentatively assigned by Fuchs, Grabisch, and Roschert to be one of the 8.274 or 8.366 or 8.933 levels. In the present experiment the 8.933-MeV level was very weakly excited (about 30 ± 10 μb/sr at 30° and 8 ± 4 μb/sr at 60° at $E_p=25$ MeV) and no angular distribution could be obtained. The 8.366-MeV level has been identified as an $L=4$ transfer in this and two (α, α') experiments. The 8.113-MeV level is taken to be $(1, 2, 3)^-$.

High L-Transfer States and Levels Above 9 MeV

Several states having spins possibly equal to 6 or greater were observed. The characteristics associated with high L transfer in the (p, p') reaction is that the angular distributions of such excited states peak at large scattering angles as can be seen in Fig. 15. The 8.191- and 8.978-MeV levels are observed with $L=6$ transfer, and their J values are tentatively assigned as 6^+. The angular distributions for the 8.850-MeV state show systematic agreement with an $L=7$ collective-model prediction at four beam energies. This state is tentatively assigned $J^\pi=(6^-)$ since this is the highest-spin, negative-parity state that can be made in any relatively simple way from the ^{40}Ca ground state. The same assignment could possibly be given to the 9.237-MeV level but with less confidence, for there is only one angular distribution analyzed and compared with theory. Further investigations by other types of reactions are needed to confirm these findings. Because of the very high density of states above 9-MeV excitation, detailed identification of states is hazardous.

Comparisons of δ_L's and G's

Table XII compares the experimental nuclear deformations, δ_L, we obtained with those from previous experiments. For six beam energies and three independent experiments, the deformation for the 3.736-MeV (3^-) state was found to be more or less a constant 1.4 F. The observations of two (α, α') measurements disagree with each other primarily due to differences in analysis. The higher-energy α data were analyzed using the Blair-Austern model, whereas the lower-energy data were analyzed using DWBA.

It appears that the deformations extracted at higher energy are consistently smaller than those at lower energies in both (p, p') and (α, α') experiments. This trend of energy dependence may result from the model and analysis procedure used.

A comparison of the reduced transition probabilities with (e, e') and γ-decay experiments is made in Table XIII. Only those transitions with 100% to ground-state branching, i.e., $B(EL; 0 \rightarrow L)$ are compared. As can be seen from the table, the G values obtained in this experiment agree very well with the majority of all other results, especially those of Eisenstein *et al.*[10] It has been pointed out by these authors that their findings are relatively parameter- or model-independent.

A comparison of $B(pp'; 0 \rightarrow L)$ and $B(\alpha\alpha'; 0 \rightarrow L)$ is shown in Table XIV. The major discrepancies occur at high excitation energies where the (α, α') results are seen to be consistently high except for the 4.491-MeV state. This is believed to be in part due to the fact that α scattering was done with less resolving power.

The reduced transition probabilities $B(EL)$ scaled for the (p, p') experiment were obtained using Fermi-equivalent uniform-density distributions.

TABLE XIV. Comparisons of reduced transition probabilities between (p, p') and (α, α').

E^* (MeV)	L	G_L (s.p.u.) (p, p') This work	(α, α') [a]
3.90	2	2.05 ± 0.20	2.9 ± 0.5
5.62	2	0.13 ± 0.05	0.7 ± 0.2
7.87	2	0.92 ± 0.15	1.8 ± 0.4
8.10	2	0.38 ± 0.06	2.1 ± 0.3
3.73	3	28.7 ± 3.0	23.6 ± 3.5
6.29	3	3.1 ± 0.3	6.6 ± 1.0
6.58	3	2.5 ± 0.3	3.8 ± 0.6
7.94	4	2.2 ± 0.2	5.6 ± 0.8
8.38	4	2.0 ± 0.2	4.3 ± 0.6
4.49	5	20.6 ± 2.1	17.7 ± 2.7

[a] Reference 7. Also in *Advances in Nuclear Physics*, edited by M. Baranger and E. Vogt (Plenum, New York, 1970), Vol. III.

VII. SUMMARY

The angular distributions for protons inelastically scattered from various excited states of ^{40}Ca have been measured at incident proton energies of 25, 30, 25, and 40 MeV. Data for about 50 states have been analyzed and the systematic and consistent variations of the distributions with respect to the proton beam energy were observed. The L transfer for most of the observed states has been compared with the results of other experiments. Good agreement was obtained in general and some ambiguities that existed in previous experiments were clarified. It is concluded that the (p, p') experiment, performed at relatively high proton energies with a good-resolution detection system, enables one to determine the L value with less uncertainty. States with spin transfer larger than 5 have been observed and identified.

The DWBA collective-model analysis has been carried out and the deformations δ_L's were extracted. It was found that the collective model was successful in predicting angular distributions in agreement with this experiment, except for the cases of $L = 0$ and $L = 1$, where it is known to be an incorrect description. Generally speaking, the collective DWBA distributions follow the same energy-dependence patterns as those of the experimental observations. It also appears that the overall shape and magnitude of the experimental angular distributions of a given L are roughly independent of excitation energy. Therefore, the δ's extracted are more or less energy-independent. However, this statement does not apply to every excited state. For example, the individual distributions of the 6.751-MeV state coincide in shape with those of the 3.736-MeV state, but the relative magnitudes in going from one energy to the next do not. Thus the observed energy dependence of δ for this 6.751-MeV state may be real and interpretations for this phenomenon are to be desired.

Finally, the ADW calculations have been performed for some negative-parity states, using the KK force and Kuo's RPA wave functions. The particle-hole configurations of these states were investigated by examining the over-all results of these ADW calculations and comparing them with other theoretical and experimental results. The nature of the states under study are fairly well understood. It was also found that the central force used in the ADW calculations is adequate in predicting the distributions of the normal-parity states, but a noncentral force may be essential to reproduce those of the unnatural-parity states.

ACKNOWLEDGMENTS

We would like to express our gratitude to all of the staff at the Michigan State University Cyclotron Laboratory for making this work possible. In particular we wish to express thanks to our colleagues, Professor S. Austin, Professor G. Bertsch, Professor G. Crawley, Professor W. Kelly, and Professor H. Wildenthal for their many invaluable discussions and comments.

†Work supported in part by the National Science Foundation.

*On sabbatical leave to CERN, Genève, Switzerland.

‡Submitted in partial requirement for Ph.D. degree. Present address: Department of Physics, Sloan-Kettering Institute, New York, New York.

§Present address: Department of Environmental Medicine, Mt. Sinai School of Medicine, New York, New York.

¶Present address: Lawrence Radiation Laboratory, University of California, Berkeley, California 94720.

‖Present address: Physics Department, University of South Carolina, Columbia, South Carolina 29208.

[1]V. Gillet and E. A. Sanderson, Nucl. Phys. 54, 472 (1964).

[2]V. Gillet and E. A. Sanderson, Nucl. Phys. A91, 292 (1967).

[3]T. T. S. Kuo and G. E. Brown, Nucl. Phys. 85, 40 (1966).

[4]W. J. Gerace and A. M. Green, Nucl. Phys. A113, 641 (1968).

[5]H. P. Leenhouts, Physica 35, 290 (1967).

[6]A. E. L. Dieperink, H. P. Leenhouts, and P. J. Brussaard, Nucl. Phys. A116, 555 (1968).

[7]E. P. Lippincott and A. M. Bernstein, Phys. Rev. 163, 1170 (1967); E. P. Lippincott, Ph.D. thesis, Massachusetts Institute of Technology, 1967 (unpublished).

[8]A. Springer and B. G. Harvey, Phys. Letters 14, 116 (1965).

[9]D. Blum, P. Barreau, and J. Bellieard, Phys. Letters 4, 109 (1963).

[10]R. A. Eisenstein, D. W. Madsen, H. Theissen, L. S. Cardman, and C. K. Bockelman, Phys. Rev. 188, 1815 (1967).

[11]K. K. Seth, J. A. Biggerstaff, P. D. Miller, and G. R. Satchler, Phys. Rev. 164, 1450 (1967).

[12]H. Fuchs, K. Grabisch, and G. Roschert, Nucl. Phys. A129, 545 (1969).

[13]A. Tellez, R. Ballini, J. Delannay, and J. P. Fonan, Nucl. Phys. A127, 438 (1969).

[14]H. G. Blosser, Commun. Electron. 52, 814 (1961).

[15]H. G. Blosser and A. I. Galonsky, IEEE Trans. Nucl. Sci. NS-13, No. 4, 466 (1966).

[16]M. M. Gordon, R. E. Berg, and H. G. Blosser, Nucl. Instr. Methods 58, 327 (1968).

[17]G. H. Mackenzie, E. Kashy, M. M. Gordon, and H. G. Blosser, IEEE Trans. Nucl. Sci. NS-14, No. 3, 450 (1967).

[18]J. L. Snelgrove and E. Kashy, Nucl. Instr. Methods 52, 153 (1967).

[19]W. Benenson, R. deForest, W. P. Johnson, and E. Kashy, Nucl. Instr. Methods 64, 40 (1968).

[20]K. Thompson, Ph.D. thesis, Michigan State University, 1969 (unpublished).

[21]C. R. Gruhn, T. Kuo, C. Maggiore, B. Preedom, L. Samuelson, and J. Chander, IEEE Trans. Nucl. Sci. 15, No. 3, 337 (1968).

[22]L. H. Johnston and D. A. Swenson, Phys. Rev. 111, 212 (1958).

[23]L. N. Blumberg, E. E. Gross, A. van der Woude, A. Zucker, and R. H. Bassel, Phys. Rev. 147, 812 (1966).

[24]J. M. Cameron, University of California, Los Angeles, California Technical Report No. P-80, 1967 (unpublished); Phys. Rev. 167, 908 (1968).

[25]B. W. Ridley and J. F. Turner, Nucl. Phys. 58, 497 (1964).

[26]J. F. Janni, Air Force Weapons Laboratory Report No. AFWL-TK-150, 1966 (unpublished).

[27]M. A. Grace and A. R. Poletti, Nucl. Phys. 78, 273 (1966).

[28]A. R. Poletti, A. D. W. Jones, J. A. Becker, and R. E. McDonald, Phys. Rev. 181, 1606 (1969).

[29]K. W. Dolan and D. K. McDaniels, Phys. Rev. 175, 1446 (1968).

[30]G. R. Satchler, Nucl. Phys. 55, 1 (1964).

[31]G. R. Satchler, Nucl. Phys. A100, 481 (1967).

[32]B. M. Preedom, C. R. Gruhn, T. Y. T. Kuo, and C. J. Maggiore, Phys. Rev. C 2, 166 (1970).

[33]M. P. Fricke, E. E. Cross, B. J. Morton, and A. Zucker, Phys. Rev. 156, 1207 (1967).

[34]R. H. Bassel, R. M. Drisko, and G. R. Satchler, Oak Ridge National Laboratory Report No. ORNL-3240, 1962 (unpublished); and Oak Ridge National Laboratory Memorandum to the Users of the Code JULIE, 1966 (unpublished).

[35]G. R. Satchler, private communication with C. R. Gruhn.

[36]G. E. Brown and A. M. Green, Nucl. Phys. 75, 410 (1966).

[37]W. J. Gerace and A. M. Green, Nucl. Phys. A93, 110 (1967).

[38]K. A. Amos, V. A. Madsen, and I. E. McCarthy, Nucl. Phys. A94, 103 (1967).

[39]R. Schaeffer, Nucl. Phys. A132, 186 (1969).

[40]F. Petrovich, H. McManus, V. A. Madsen, and J. Atkinson, Phys. Rev. Letters 22, 895 (1969).

[41]T. T. S. Kuo, private communication with H. McManus.

[42]F. Petrovich, Ph.D. thesis, Michigan State University, 1970 (unpublished).

[43]W. G. Love and G. R. Satchler, Nucl. Phys. A159, 1 (1970).

[44]S. M. Perez, Nucl. Phys. A136, 599 (1969).

[45]J. R. Erskine, Phys. Rev. 149, 854 (1966).

[46]P. Goode, Nucl. Phys. A140, 481 (1970).

[47]S. M. Austin, R. Schaeffer, and W. Benenson, private communication with C. R. Gruhn.

[48]W. J. Gerace and A. M. Green, Nucl. Phys. A123, 241 (1969).

[49]P. Federman and S. Pittel, Nucl. Phys. A139, 108 (1969).

[50]P. Federman and S. Pittel, Phys. Rev. 186, 1106 (1969).

[51]R. Anderson, A. G. Robertson, D. F. H. Start, L. E. Carlson, and M. A. Grace, Nucl. Phys. A131, 113 (1969).

[52]S. M. Smith and A. M. Bernstein, Nucl. Phys. A125, 339 (1969).

[53]C. Glashausser, M. Kondo, M. E. Rickey, and E. Rost, Phys. Rev. Letters 14, 113 (1965).

[54]R. Paddock, Ph.D. thesis, Michigan State University, 1969 (unpublished).

[55]A. Marinov and J. R. Erskine, Phys. Rev. 147, 826 (1966).

[56]J. R. MacDonald, D. F. H. Start, R. Anderson, A. G. Robertson, and M. A. Grace, Nucl. Phys. A108, 6 (1968).

[57]H. P. Leenhouts and P. M. Endt, Physica 32, 322 (1966).

[58]H. Lindeman, G. A. P. Engelbertink, M. W. Ockeleon, and H. S. Pruys, Nucl. Phys. A122, 373 (1968).

[59]F. R. Metzger, Phys. Rev. 165, 1245 (1968).

[60]W. S. Gray, R. A. Kenefick, and J. J. Kraushaar,

Nucl. Phys. 67, 542 (1965).
[61]J. S. Forster, K. Bearpark, J. L. Hutton, and J. F. Sharpey-Schafer, Nucl. Phys. A150, 30 (1970).
[62]H. A. Enge, E. J. Irvin, and D. H. Weaner, Phys. Rev. 115, 949 (1959).
[63]M. E. Rickey, E. Kashy, and D. Knudsen, Bull. Am. Phys. Soc. 10, 550 (1965).
[64]E. Kashy and J. L. Snelgrove, Phys. Rev. 172, 1124 (1968).
[65]K. Yagi *et al.*, Phys. Letters 10, 186 (1964).

PHYSICAL REVIEW C VOLUME 6, NUMBER 3 SEPTEMBER 1972

Proton Inelastic Scattering from $^{48}Ca^{\dagger}$

C. R. Gruhn,* T. Y. T. Kuo,‡ C. J. Maggiore,§ and B. M. Preedom¶
Department of Physics and Cyclotron Laboratory, Michigan State University, East Lansing, Michigan 48823
(Received 29 December 1971)

Inelastic proton scattering from ^{48}Ca has been measured at beam energies 25, 30, 35, and 40 MeV. Angular distributions from 13 to 97° for 22 inelastic states were obtained. Analyses with the collective distorted-wave Born approximation are presented. A direct comparison of the excitation of the ^{48}Ca 3.830-MeV 2^+ and 6.342-MeV 4^+ states is made with the low-lying excited 2^+ and 4^+ states of ^{50}Ti and ^{52}Co.

I. INTRODUCTION

Doubly magic nuclei, in general, have been studied in great detail both experimentally and theoretically. Perhaps the exception to this statement is ^{48}Ca. From the experimental standpoint only a few of the low-lying states of ^{48}Ca have well established spin and parity. From the theoretical point of view ^{48}Ca is of interest because of the purity of its double-closed-shell structure. Jaffrin and Ripka[1] have tested the occupation numbers and find that the $1f_{7/2}$ shell and the inner neutron shells are at least 97% closed. It is because of the strong theoretical motivation and of our interest in developing the (p,p') reaction as a probe in microscopic structure that we undertook the present (p,p') experiment on ^{48}Ca.

The level structure of ^{48}Ca has also been investigated in other experiments such as (α, α'),[2,3] (e, e'),[4] (t,p),[5] (p,p'),[6] and $(p,p'\gamma)$.[7] The (α, α') and (e, e') experiments probably should be repeated with the now available better resolutions. In principle, then, at least some of the ambiguities in the present assignments of the low-lying levels could be removed.

II. DESCRIPTION OF EXPERIMENT

The experiment was carried out using the proton beam from the Michigan State University sector-focused cyclotron. Figure 1 shows the cyclotron and beam-handling system. The two horizontal bending magnets M3 and M4 are used to momentum analyze the beam and M5 deflects the beam into the goniometer.[8] More complete descriptions of the properties of the energy analysis system have been published elsewhere.[9,10] During this experiment the slits S1 and S3 were set at 15 mils for beam energy resolution of ±5 keV. S2 was set at 100 mils to yield a beam divergence of ±2 mrad. The Faraday cup is located in a shielded beam dump 12 ft beyond the goniometer.

The scattered protons were detected with two surface-barrier Ge(Li) detectors designed specifically for this experiment.[11] The two detectors were separated by 14.7° and were located outside the 16-in. scattering chamber. The detectors coupled to the scattering chamber vacuum via a sliding seal. A monitor counter at a fixed angle viewed the scattered beam through a 1-mil Kapton window.

The target was a commercially prepared self-supporting foil of ^{48}Ca approximately 1.08 mg/cm^2 thick. The composition of the target as determined by the Isotopes Division of Oak Ridge National Laboratory is listed in Table I. The target was stored in vacuum when not in use and transferred to the scattering chamber in vacuum via a target-transfer system.[8]

Inelastic proton spectra were taken every 5° from 13 to 97°. The over-all energy resolution was 25–30 keV full width at half maximum. Each counter subtended an angle of about 0.5° in the scattering plane. The scattering angle was checked by comparing the positions of the H and ^{12}C contaminant peaks relative to the ^{48}Ca ground state and found to be accurate to within 0.1°. The energy of the incident protons determined by mea-